Tectonophysics 491 (2010) 253–274

Contents lists available at ScienceDirect

Tectonophysics

journal homepage: www.elsevier.com/locate/tecto

Spatial distribution of denudation in Eastern Tibet and regressive erosion of plateau margins

V. Godard [a,b,*], J. Lavé [c,d], J. Carcaillet [d], R. Cattin [b,e], D. Bourlès [a], J. Zhu [f]

[a] CEREGE, CNRS-UMR6635, Aix-Marseille Université, Aix-en-Provence, France
[b] Laboratoire de Géologie, CNRS-UMR8538, Ecole Normale Supérieure, Paris, France
[c] CRPG, CNRS-UPR2300, Vandoeuvre-Lès-Nancy, France
[d] GCA, CNRS-UMR5025, Université Joseph Fourier, Saint-Martin d'Hères, France
[e] Géosciences Montpellier, CNRS-UMR5243, Université Montpellier 2, Montpellier, France
[f] Chengdu University of Technology, Chengdu, China

ARTICLE INFO

Article history:
Received 13 February 2009
Accepted 29 October 2009
Available online 5 November 2009

Keywords:
Eastern Tibetan Plateau
Cenozoic
Denudation processes
Topographic margin evolution
Wenchuan earthquake

ABSTRACT

The Longmen Shan range is one of the major topographic and structural features of the eastern margin of the Tibetan Plateau. With an impressive topographic gradient and low convergence rates across the range this region has raised important questions concerning the dynamics of plateau margin settings, such as the long-term mechanisms of topographic evolution. The investigation of the distribution in space and time of denudation can provide critical insight into such dynamics and shed light on still unresolved controversies. For that purpose, we present a new dataset that documents the intensity and distribution of denudation processes across this plateau margin through field survey of fluvial incision markers, quantitative geomorphology and cosmogenic nuclide derived basin-wide erosion rates. Erosion is <0.5 mm/year in the frontal region of the Longmen Shan and between 0.5 and 1 mm/year further west, with a gradual decrease when reaching the northern headwaters of the Min Jiang watershed, adjacent to the beginning of the Tibetan Plateau. The spatial distribution of denudation inferred from the various methods we use suggests that most of the differential uplift in the Central Longmen Shan is accommodated by the Beichuan Fault and frontal structures located in the foothills. The denudation pattern seems also to reflect the large-scale propagation of erosion from the Sichuan Basin toward the Plateau. This suggests that the Longmen Shan range is submitted to the combined influences of slow thrusting activity on the frontal structures and progressive westward regressive erosion as a probable response to a pulse of uplift of the Tibetan Plateau Eastern margin, that started 10 Ma ago.

1. Introduction

The broad Himalayan-Tibet collision zone has attracted a host of studies over the last 30 years (Molnar and Tapponnier, 1975; Armijo et al., 1986; England and Houseman, 1989; Coleman and Hodges, 1995; An et al., 2001). It is indeed the most impressive geodynamical and topographical feature on Earth (Fielding et al., 1994), and presents areas of vigorous activity for both tectonics and surface processes (Burbank et al., 1996; Lavé and Avouac, 2000; Avouac, 2003). It provides an exceptional natural laboratory for the testing and evaluation of new concepts for lithospheric dynamics, related to tectonics, denudation and their potential linkages in such actively deforming settings (Cattin and Avouac, 2000; Beaumont et al., 2001). However, the large-scale picture of the geodynamic evolution of this region is not yet resolved, and several controversies remain concerning the modalities of plateau building in the late Cenozoic (Royden et al., 1997; Tapponnier et al., 2001; Zhang et al., 2004; Thatcher, 2007; Royden et al., 2008; Liu-Zeng et al., 2008) and their eventual coupling with climate evolution (Raymo and Ruddiman, 1992; Molnar et al., 1993; Hay et al., 2002). The Eastern Tibet region, and in particular the Longmen Shan range, have been under close scrutiny over the last decade (Burchfiel et al., 1995; Royden et al., 1997; Kirby et al., 2002; Clark et al., 2004).

Attention of researchers was attracted by the paradoxical combination of high topographic gradients with very low convergence rates across the range. Indeed, the Longmen Shan presents an impressive topographic step, with an abrupt transition between the low-elevation Sichuan Basin and the high Tibetan Plateau, and a regional gradient comparable to what is observed in the Himalayas (Clark and Royden, 2000). Despite this, no significant shortening had been documented by GPS studies across the range during the last decade (King et al., 1997; Chen et al., 2000; Gan et al., 2007), casting some doubt about this steep topographic margin being sustained by thrust tectonic activity. Several geodynamical models have been proposed to explain this peculiar configuration (Tapponnier et al., 2001; Clark et al., 2005; Wilson et al.,

* Corresponding author. CEREGE, CNRS-UMR6635, Aix-Marseille Université, Aix-en-Provence, France.
E-mail address: godard@cerege.fr (V. Godard).

0040-1951/$ – see front matter © 2009 Elsevier B.V. All rights reserved.
doi:10.1016/j.tecto.2009.10.026

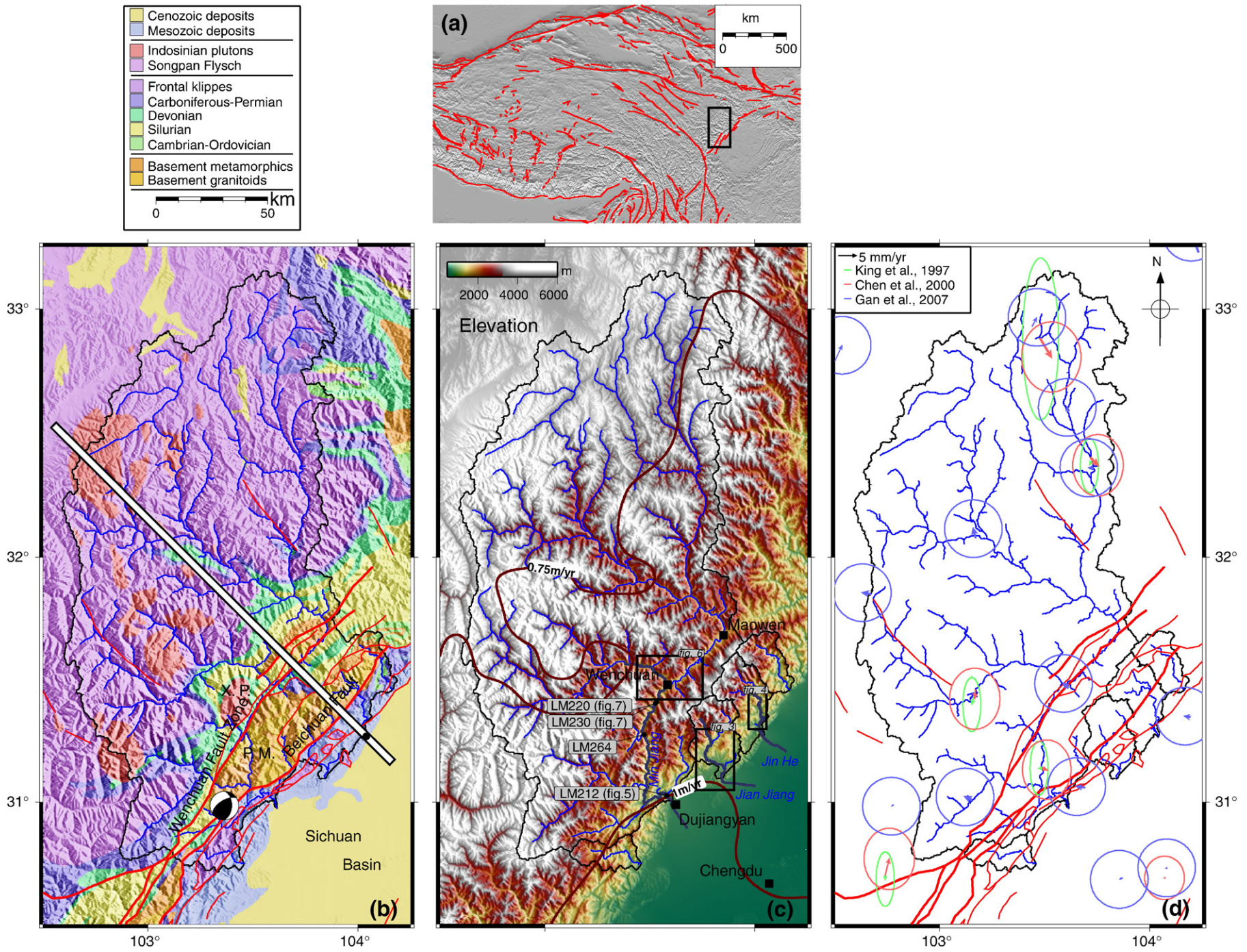
Cenozoic deposits
Mesozoic deposits
Indosinian plutons
Songpan Flysch
Frontal klippes
Carboniferous-Permian
Devonian
Silurian
Cambrian-Ordovician
Basement metamorphics
Basement granitoids
km
0
50
(a)
km
0
500
33°
32°
31°
103°
104°
(b)
H. P.
P.M.
Wenchuan Fault Zone
Beichuan Fault
Sichuan
Basin
m
2000 4000 6000
Elevation
0.75m/yr
Maowen
Wenchuan
fig. 6
fig. 4
fig. 3
LM220 (fig.7)
LM230 (fig.7)
LM264
LM212 (fig.5)
1m/yr
Min Jiang
Jin He
Jian Jiang
Dujiangyan
Chengdu
(c)
5 mm/yr
King et al., 1997
Chen et al., 2000
Gan et al., 2007
N
(d)

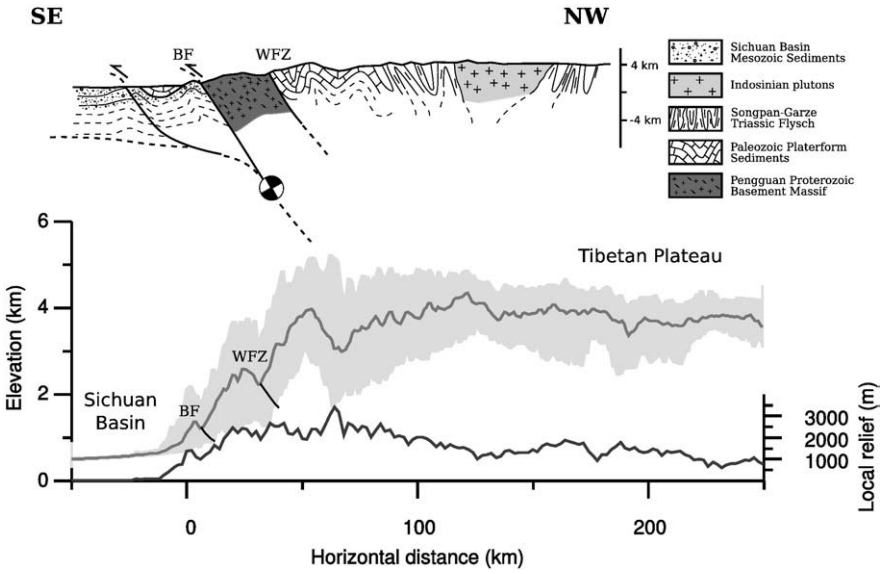

Fig. 2. Schematic geological cross section across the Central Longmen Shan, perpendicular to the strike of the range (adapted from Burchfiel et al. (1995). The focal mechanism for the May 12th earthquake is indicated. Corresponding topography from GTOPO30 dataset (mean and extreme values) and local relief profile (40 km swath width). WFZ Wenchuan Fault Zone, BF Beichuan Fault.

2006; Hubbard and Shaw, 2009), but further discussion of their relevance require additional documentation on the evolution of tectonics and denudation processes in space and time, as well as the acknowledgement that the recent Sichuan earthquake demonstrated that thrust activity is still an on-going process.

It is a classical conception in geomorphology that landscapes result from an interaction between internal tectonic processes, and external denudation processes (e.g. Beaumont et al., 1992; Willett and Brandon, 2002; Whipple and Meade, 2004). It conveys the idea that the amplitude and distribution of erosion are chiefly modulated by those of tectonic uplift, with high uplift settings commonly associated with high denudation. For that reason, the analysis of the modalities and distribution of erosion in Eastern Tibet can provide critical insights to understand tectonic processes at work in that area.

The purpose of this study is to document active denudation, in terms of rates and processes, across the Central Longmen Shan, in order to put constraints on the geodynamical evolution of this region. We first review the most important geological and morphological features of this mountain range, and then, we present a selection of field sites that provide relevant elements for the assessment of the fluvial incision rates and processes. On this basis, we attempt to capture the relative spatial variations in erosion, by computing fluvial shear stress acting along major rivers and analysing its relation with underlying lithology. We then compare this pattern of fluvial incision, with estimates of Late Holocene landscape erosion, obtained from cosmogenic nuclide concentrations in alluvial sands. Lastly, a synthesis of our different estimates for denudation rates is used to evaluate tectonic scenarios and test the transient nature of the present erosion pattern.

2. Settings

2.1. Topography and rainfall distribution

The Longmen Shan range is located along the Eastern border of the Tibetan Plateau (Fig. 1). It accommodates a sharp topographic transition between the Sichuan Basin and the Plateau, with a shift in mean elevation from ~500 m to ~4000 m in less than 60 km of horizontal distance. From east to west, one first encounters a narrow range of frontal hills, along the western edge of the Sichuan Basin, that is abruptly followed by the topographic front of the range, with deep gorges and summit above 5000 m. Further west, entrenchment gradually decreases when approaching the low relief Tibetan Plateau (Kirby et al., 2003).

The distribution of precipitations in Eastern Tibet is controlled by two dominant factors, the southeast Asia monsoon and the orographic effect associated with the topographic step (New et al., 2002). With a decrease in precipitation rates from ~1 m/year on the basin, to ~0.7 m/year on the Plateau, the rain shadow appears modest when compared to other regions such as the Himalayas (Bookhagen and Burbank, 2006). Most of the precipitation is concentrated during the summer months, with a monsoon effect more pronounced on the Basin than on the Plateau.

2.2. Geology of the Longmen Shan

The Longmen Shan range marks the geologic transition between the low-elevation Sichuan basin and the Tibetan Plateau. It has a complex structure resulting from a polyphase history. From east to west the following tectono-stratigraphic units are successively observed (Figs. 1b and 2).

The easternmost frontal units of the range are made of Mesozoic detrital sediments, which mainly consist of sandstone and siltstone of Triassic to Jurassic age characterized by thin-skinned fold and thrust deformation (Chen and Wilson, 1996). Those sediments belong to the thick Meso-Cenozoic continental detrital series of the Sichuan Basin (Burchfiel et al., 1995), constituting the foreland of the Longmen Shan. The limited Late Cenozoic sedimentation in this basin suggests an absence of significant flexural loading associated with recent thrusting activity along the Longmen Shan by the easternmost faults such as the Beichuan Fault (Royden et al., 1997).

Fig. 1. (a) Tibetan Plateau shaded relief map with the location of insets (b–d). (b) Geological map of the Central Longmen Shan. The focal mechanism for the May 12th 2008 Eastern Sichuan earthquake is shown (USGS). Approximate orientation of the cross section presented on Fig. 15 is also indicated. P. M. — Pengguan Massif. X. P. — Xuelongbao Pluton. (c) Topographic map of the Central Longmen Shan, with location of the surveyed sites. The dark red contours are precipitation data from New et al. (2002). The portions of Jian Jiang, Jin He and Min Jiang rivers described in Figs. 9 and 10 are indicated in dark blue. (d) GPS velocities in a fixed Sichuan Basin reference frame (95% confidence).

The basement core of the Proterozoic granitoids and metamorphic (metavolcanics and metasediments) rocks of the Yangtze craton, such as the Pengguan Massif, constitutes the highest part of the range (Burchfiel et al., 1995; Chen and Wilson, 1996). These are the oldest formations encountered in this part of Eastern Tibet, and have an important role in shaping the morphology of the abrupt topographic front. The main structural features of the Central Longmen Shan are the Wenchuan and Beichuan faults that bound the Pengguan Massif on its western and eastern flank, respectively.

During most of the Paleozoic times the western part of the Yangtze craton was a passive margin, accumulating an important sedimentary platform sequence. This series is mainly constituted by shallow water detrital deposits (sandstone and shales) and limestone. From a structural point of view those units are directly deposited on the Proterozoic basement blocks and mark the transition between the Longmen Shan and the Songpan Garze fold belt. As a whole the series underwent low grade (green schist) metamorphism. Those sediments are also present in the frontal part of the range as klippes overlying the Mesozoic formations of the Sichuan Basin.

The Songpan Garze sequence was deposited during Triassic and overtops the Paleozoic platform sequence described above. It consists mainly of detrital sediments of flysch facies. The series is intensely folded (Harrowfield and Wilson, 2005) and underwent moderate metamorphism, whose grade increases westward (Wallis et al., 2003). Those sediments are intruded by several granitic plutons, contemporary with the main Indosinian (late Triassic) deformation stage (Mattauer et al., 1992; Worley and Wilson, 1996; Harrowfield and Wilson, 2005).

2.3. Tectonic evolution

2.3.1. Long-term evolution documented by thermochronology

The evolution of the Longmen Shan results from a complex history, with successive tectonic episodes during the Indosinian and Himalayan orogenic cycles (Burchfiel et al., 1995; Huang et al., 2003; Harrowfield and Wilson, 2005; Wilson et al., 2006). Low-temperature thermochronology has documented a major exhumation episode starting at ~10 Ma (Arne et al., 1997; Kirby et al., 2002; Godard et al., 2009a), but the activity of the major structures of the range during the late Cenozoic is still debated (Densmore et al., 2007).

The Wenchuan Fault Zone is an inherited structure from the network of normal faults of the Paleozoic passive margin, and was reactivated under a transpressive tectonic regime during subsequent orogenic cycles (Burchfiel et al., 1995). However, as pointed out by Godard et al. (2009a), no significant dip slip activity was accommodated by this structure over the last 10 Ma. Conversely, it has been shown that thrusting across the Beichuan Fault has chiefly contributed to the exhumation of the Pengguan Massif, with a long-term slip rate of 0.4–1 mm/year since 10 Ma, as inferred from the position of the 180 °C paleo-isotherm (Godard et al., 2009a). Farther east, the activity of the frontal fault system is more difficult to assess on the basis of thermochronology, but compilation of available data suggests subdued activity across those structures (Arne et al., 1997; Richardson et al., 2008; Godard et al., 2009a).

In addition, comparison of apatite and zircon ages across the Pengguan Massif indicates that the easternmost part has probably experienced a recent ~2 fold decrease in exhumation rate. This would suggest that the peak of denudation initiated at 10 Ma has shifted in this part of the range toward more subdued erosion conditions, and was interpreted by Godard et al. (2009a) as a result of the propagation of a transient westward wave of regressive erosion.

2.3.2. Quaternary deformations and seismotectonic regime

Due to the apparent lack of flexure of the Sichuan Basin, the amount of thrusting activity across the Beichuan Fault and the easternmost Pengguan fault has been questioned. Both faults present evidence supporting late Pleistocene and even Holocene activity in some sites (Densmore et al., 2007), however the exact amount of cumulative slip remains poorly constrained. Densmore et al., (2007) report a dominantly dextral slip activity on those structures, with a late Quaternary throw rate <1 mm/year.

More than a decade of GPS campaigns in Eastern Tibet associated with regular measurements of the Chinese geodetic networks indicate that no significant shortening across the Longmen Shan, between the Tibetan Plateau and the Sichuan Basin, was resolvable within the 2σ confidence intervals (King et al., 1997; Chen et al., 2000; Zhang et al., 2004; Gan et al., 2007) (Fig. 1d).

Nevertheless, the area is seismically active, with a localization of historical events and microseismicity along the Longmen Shan range (Yang et al., 2005). Despite these slow convergence and stress accumulation rates, the recent M_w ~ 7.9, May 2008, Sichuan Event has shown the potential of the frontal structures of the Longmen Shan to generate major earthquakes, and clearly demonstrates that thrusting activity on the Beichuan Fault, as seen by the paleo-isotherm offset since 10 Ma on both sides of this fault, is still an on-going process (Godard et al., 2009a). Seismological and geodetic data do not permit, for the moment, to document if the present thrusting rate on the Beichuan Fault equals the average long term, nor they permit to assess the tectonic activity of the most frontal folds. In particular Densmore et al. (2007) observations document also a dominant strike slip component on these faults. Contrastingly, field mapping of the rupture carried out in the aftermath of the 2008 earthquake indicates a roughly equivalent amount of thrust and right lateral slip on the Beichuan fault and dominant thrust slip on the Pengguan fault (Dong et al., 2008; Liu-Zeng et al., 2009; Lin et al., 2009). This could reflect either a significant change in the slip pattern from one major earthquake to another or the difficulty to observe thrusting activity due to the poor preservation of corresponding geomorphologic markers.

In order to improve our understanding of the recent vertical motion and potential fault and fold activities, we consider in the following spatial pattern and rates of erosion across the Longmen Shan as an indicator of underlying tectonic activity.

3. Fluvial terraces, incision and erosion processes in the Central Longmen Shan

Here we report our observations of the intensity and nature of fluvial incision processes in order to highlight some features of the tectonic regime at work in the Longmen Shan. We focus on small catchments draining the frontal range, on the eastern flank of the Pengguan Massif, and along the lower reach of the Min Jiang river (Fig. 1).

3.1. Frontal range

Well developed terrace levels are cut in the Mesozoic detrital units, east of the Beichuan Fault, along the small frontal rivers and the Min Jiang.

3.1.1. Jian Jiang

The Jian Jiang is the main river of one of the small frontal catchments draining the eastern flank of the Pengguan Massif (Fig. 3). It follows, for several kilometers, the contact between this massif and the frontal sediments, along the Beichuan Fault. Alluvial deposits are widespread along this river. Terrace levels present three distinct groups corresponding to successive emplacements of fill deposits. The oldest strath surfaces are up to ~40 m above the present river, and the youngest just a few meters. Relatively few high-level terrace remnants are preserved. The thickness of the fill deposits is highly variable, ranging from 10 to 70 m but they tend to decrease downstream.

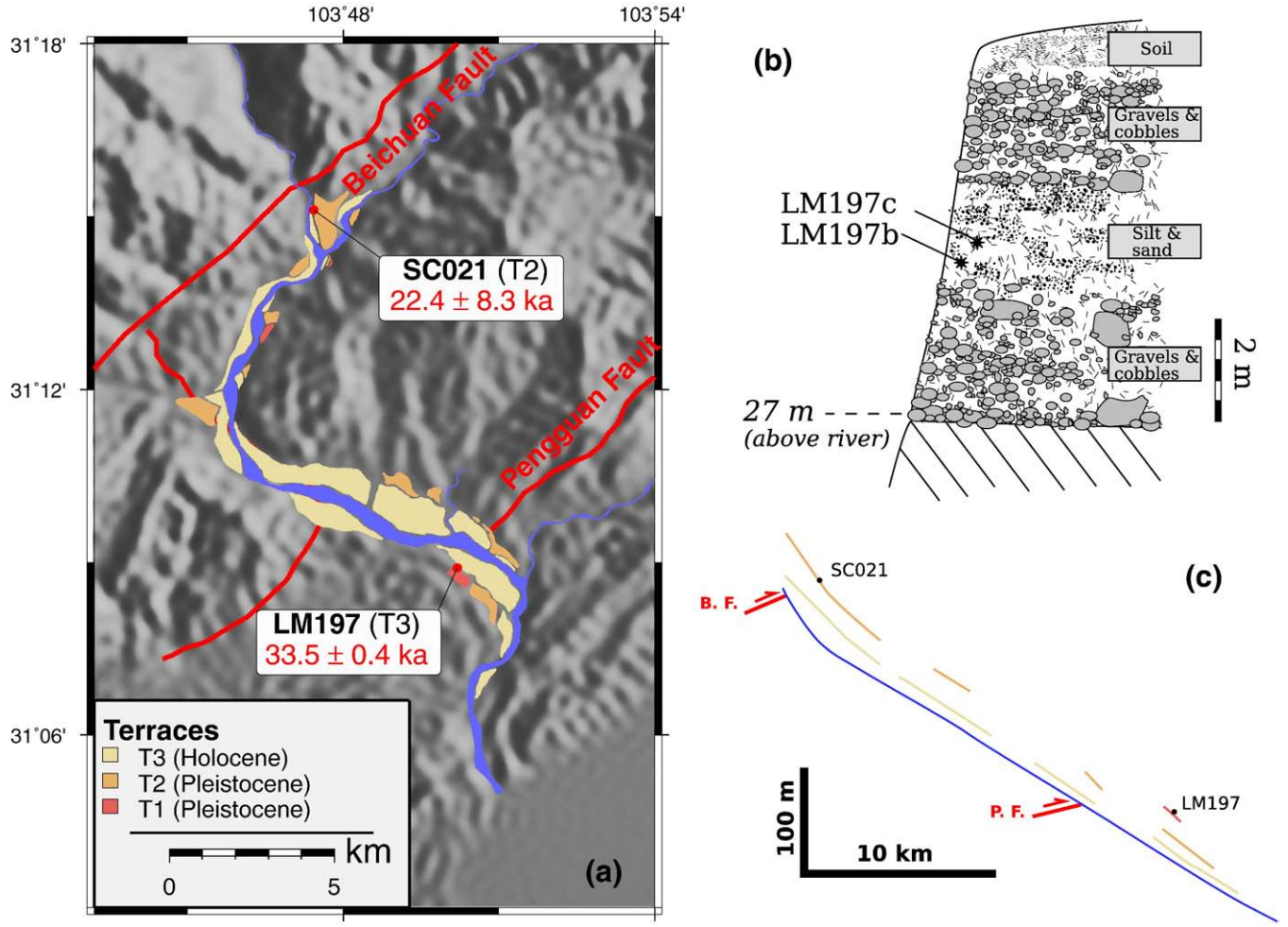

Fig. 3. (a) Distribution and geometry of Quaternary terraces along the Jian Jiang river in the frontal Longmen Shan. See Fig. 1 for situation. White cross pattern indicates the Pengguan Massif. Faults are from rupture mapping of Liu-Zeng et al. (2009). (b) Details of the fill above LM197 strath surface (with altitude above present river). (c) Along river profile of the main terraces above the Jian Jiang.

We surveyed a terrace remnant in the lower reach of the Jian Jiang (site LM197, Fig. 3). This is a narrow outcrop exposed as a nearly horizontal unconformity between bedrock and the overlying 10-to-13-meters-thick fluvial sediments of the terrace material. We interpreted it as a strath surface carved into Triassic sandstone. Charcoals were sampled in a silt and sand layer, within coarser material made of cobbles of various lithologies at its top and bottom. Those charcoals gave ages of 15.9 ± 0.4 ka BP and 33.5 ± 0.4 ka BP (Table 1). As the oldest age is associated with the deepest charcoal, presenting better indicators of preservation and protection in the fill sequence, we assume that it is the most likely to be representative of the age of the terrace emplacement. Considering that the strath surface is ~27 m above the present river, we calculate an incision rate at this location of 0.8 ± 0.2 mm/year. This rate could represent a maximum if the surveyed unconformity is not a strath, but a gentle paleo-hillslope.

Further north, a massive fill deposit is present near the confluence of the Jian Jiang with its major tributary in the footwall of the Beichuan fault (site SC021, Fig. 3). This terrace is mainly made of granitic and granodioritic boulders, from the Pengguan basement. The bedrock surface on which the fill is deposited is located ~10 m above the present river bed, immediately in the footwall of the Beichuan Fault, and present an apparent 5 m vertical offset across a branch of this fault. Further eastward this bedrock surface at the base of the fill terrace plunges toward the channel level after a few hundred meters. A massive granitic boulder was sampled on the top of the fill deposit. Cosmonuclide dating gave an apparent exposure age of ~22.4 ± 8.3 ^{10}Be ka (Table 2), assuming that inheritance is minimal. This value produces a maximum incision rate at this location of 0.4 ± 0.2 mm/year and close to 0 further downstream. Densmore et al. (2007) measured a ~4.5 m offset of this terrace by the Beichuan Fault. According to our estimation of the age this would imply a ~0.2 mm/year vertical offset rate. Similar deposits exist in other place along the Jian Jiang, but their thickness decrease downstream, from ~70 m at site SC021 to 30–40 m a few kilometers southward. Their emplacement is probably coincident with a period of increased coarse sediment delivery from the Pengguan Massif.

Table 1
Radiocarbon analyses for samples from terraces along the Jin He, Jian Jiang and Min Jiang rivers.

Sample	Material	^{14}C age (ka BP)	Calibrated/corrected age (ka BP)
LM197b	Charcoal	13.39 ± 0.10	15.9 ± 0.4
LM197c	Charcoal	29.05 ± 0.26	33.5 ± 0.4*
LM206c	Charcoal	36.80 ± 0.60	41.8 ± 0.4*
LM220c	Gasteropod shell	16.92 ± 0.08	20.1 ± 0.2
LM230	Gasteropod shell	17.54 ± 0.13	20.8 ± 0.4
LM262b	Gasteropod shell	3.30 ± 0.04	3.5 ± 0.1

Ages younger than 21 ^{14}C ka BP were calibrated using the CALIB program version 5.0 (Stuiver et al., 2005), based on the IntCal04 data set (Reimer et al., 2004). Ages older than 21 ^{14}C ka BP (* in the table) were corrected using the CALPAL-2007-HULU curve (Danzeglocke et al., 2008; Weninger and Jöris, 2008). Reported errors are 2σ.

Table 2
^{10}Be analyses for samples from terraces along the Jian Jiang and Min Jiang rivers.

Sample	Depth (cm)	^{10}Be (10^4 at/g)	Altitude (m)	Shielding factor	Age (ka)
LM264	0	2.11 ± 1.06	1158	0.76	3.5 ± 2.1
SC021	0	19.49 ± 5.24	1134	0.99	22.4 ± 8.3

^{10}Be analytical uncertainties are based on counting statistics (1σ) and a conservative assumption of 3% variability accelerator response. Production rates were calculated according to Stone (2000). We assume a 10% uncertainty on the production rates and propagate it to the final result. Production rates were also corrected for local slope and topographic shielding due to surrounding morphologies following Dunne et al. (1999). See Section 5 and Table 4 for further details on the processing of those samples.

3.1.2. Jin He

The Jin He river presents features similar to the Jian Jiang. It has its headwaters inside the Pengguan Massif, crosses the Beichuan Fault, and in its lower reaches it flows on the sedimentary units of the Sichuan Basin. Alluvial deposits are relatively scarce in its upper reach, but become more abundant downstream. As for the Jian Jiang, three levels of terraces can be observed (Fig. 4), with better preservation in the upper level.

This highest terrace level was surveyed at site LM206 (Fig. 4). A debris flow coming from a tributary of the Jin He overtops the strath surface and its fill. A charcoal sample in this debris flow was radiocarbon dated at 41.8 ± 0.4 ka BP (Table 1). This age can be interpreted as a minimal age for the emplacement of the fill sediments of the higher terrace level. Considering the difference in elevation between the strath associated with this terrace and the current river level (~57 m), it implies a maximum incision rate of 1.4 ± 0.2 mm/year at this location.

3.2. Min Jiang river

The Min Jiang is the major river of the drainage system of the Central Longmen Shan. It crosses the whole range from the Songpan flysch to the frontal units. It flows north–south from its headwaters on the Tibetan Plateau, down to the Wenchuan Fault Zone (Fig. 1). It then follows the path of the WFZ for ~60 km and then flows north–south again while crossing the Pengguan Massif until it reaches the Sichuan Basin.

3.2.1. The Min Jiang across the frontal units

East of the Beichuan Fault the Min Jiang crosses the frontal units made of Mesozoic detrital sediments locally overlain by Paleozoic klippes of platform sediments. Across this reach, the river has a characteristic width of ~100 m and it has migrated laterally abandoning numerous impaired terraces. This is particularly evident ~10 km upstream of Dujiangyan city, where a large set of terraces are preserved (Fig. 5). There, road building works have exposed a 20 m-high fresh cut in the material of one of these terraces. The base of the

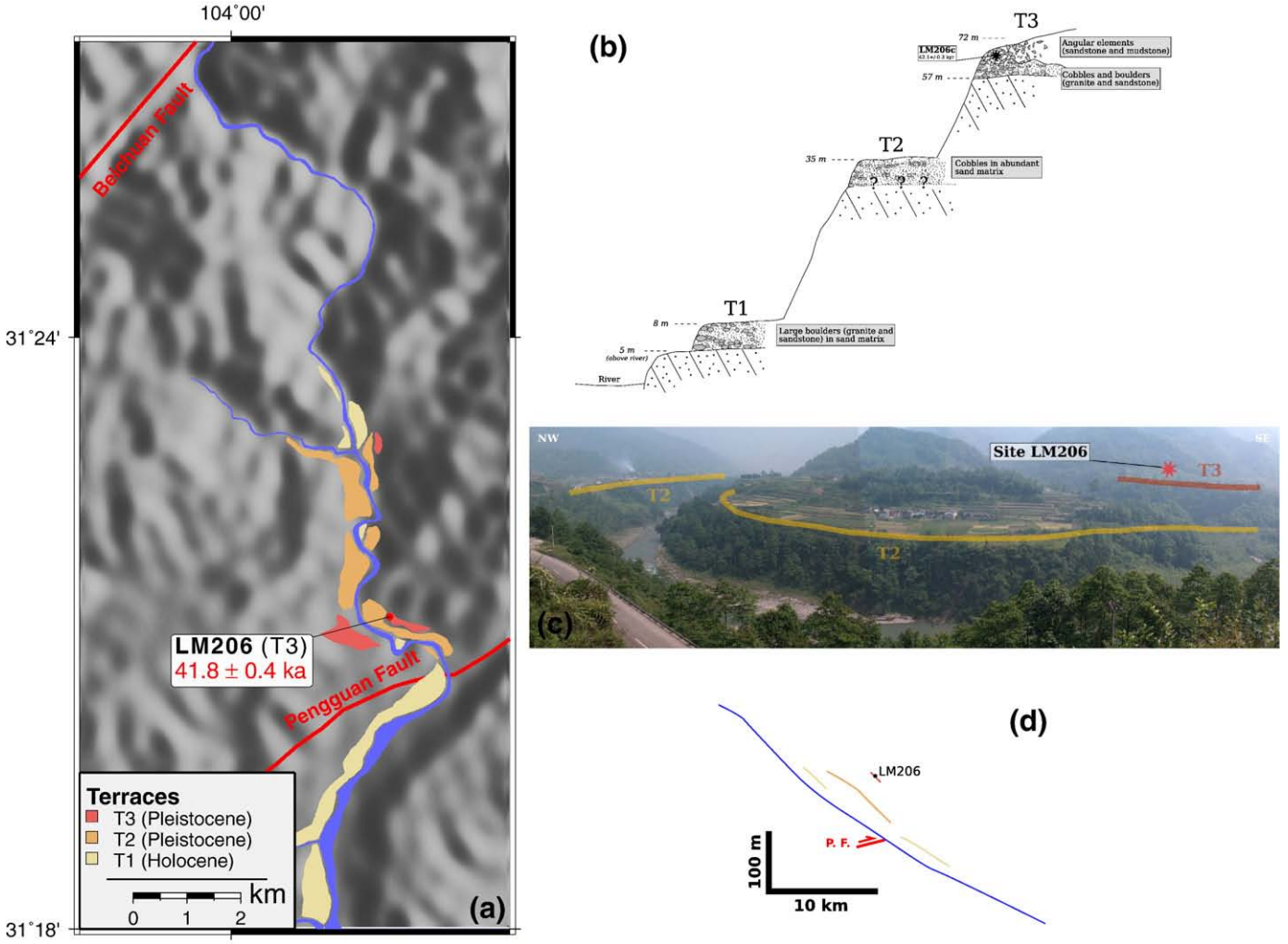

Fig. 4. (a) Distribution and geometry of Quaternary terraces along the Jin He river in the frontal Longmen Shan. See Fig. 1 for situation. White cross pattern indicates the Pengguan Massif. Faults are from rupture mapping of Liu-Zeng et al. (2009). (b) Sequence of terraces at sampling site LM206 (with altitudes above present river). (c) View on sampling site LM206 from the opposite bank of the Jin He. (d) Along river profile of the main terraces above the Jin He.

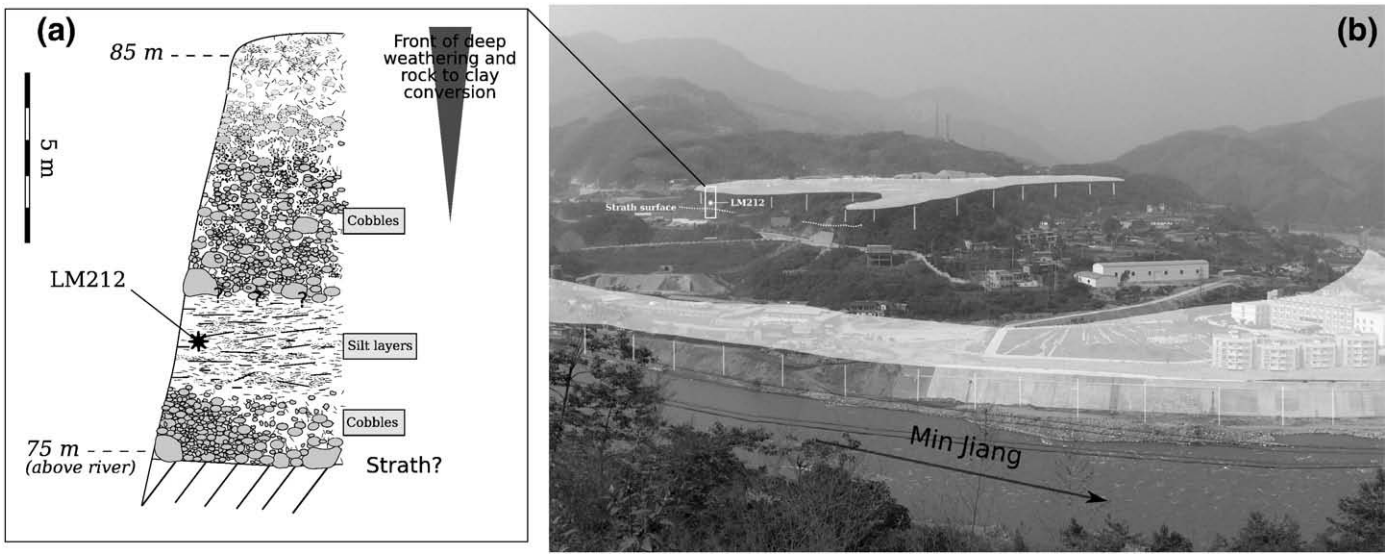

Fig. 5. (a) Description of fill sequence and sampling site for sample LM212 (with altitudes above present river). (b) Situation of site LM212. See Fig. 1 for situation.

fill is made of a coarse boulder level, overtopped by 2–3 m of silts, and then mixed levels of silts, sand and clay. The whole fill sequence is overtopped by a level of deep red-weathered cobbles and boulders. The lowermost silt sequence was sampled for OSL dating and yield an age of 150 ± 25 ka (dose rate 4.0 ± 0.4 Gy/ka, paleodose 601 ± 30 Gy, water content 15% ± 10). Considering that the strath surface associated with this terrace is 75 m above the Min Jiang, it implies that the average incision rate at that location, over the last 150 ka, is 0.5 ± 0.1 mm/year.

3.2.2. The Min Jiang between the Beichuan and Wenchuan Faults

Upstream of the Beichuan Fault, the Min Jiang channel becomes narrower, and lacks major strath terraces, in particular across the Pengguan Massif. North-west of this massif, the Min Jiang valley is characterized by the presence of numerous remnants of massive transient landslide deposits, coarse alluvial fans and lake-dammed lacustrine deposits.

In Eastern Tibet, large landslides that dammed rivers and created a lake upstream seem to be a common feature (Ouimet et al., 2007). They usually last up to several ka, until the river incises the accumulated material. A few kilometers downstream of the town of Wenchuan, we surveyed such a massive lacustrine fill associated with a landslide dam, that has been reincised by the Min Jiang river (Fig. 6). The thickness of the fill at that location (site SC037) is ~150 m. The sediments are made of fine lithic fragments, interstratified with coarser colluvial material close to the valley flanks. This formation has also been observed in several locations upstream, where it progressively includes a larger proportion of coarser fluvial material. Considering that the top of the deposit is at 1460 m asl, at site SC034, its extension reaches up to 25 km upstream in the Min Jiang valley (Fig. 6b). At site LM262, a piece of charcoal sampled in this formation was radiocarbon dated at 3.5 ± 0.1 ka BP (Table 1), and indicates that the reincision process of the landslide dam and upstream lacustrine sediments has been particularly fast.

A few kilometers downstream of the landslide that created this lake, we surveyed a deposit made of massive subangular to rounded granitic boulders with an abundant sandy matrix, which molded an ancient valley topography up to ~55 m above the present Min Jiang level (Fig. 7). The lithology of this deposit contrasts with that of the active bedload of the Min Jiang, which is dominated by quartzites and metabasites, with relatively few granitoids. This indicates that this fill sequence is a debris fan fed by a tributary draining a nearby granitic

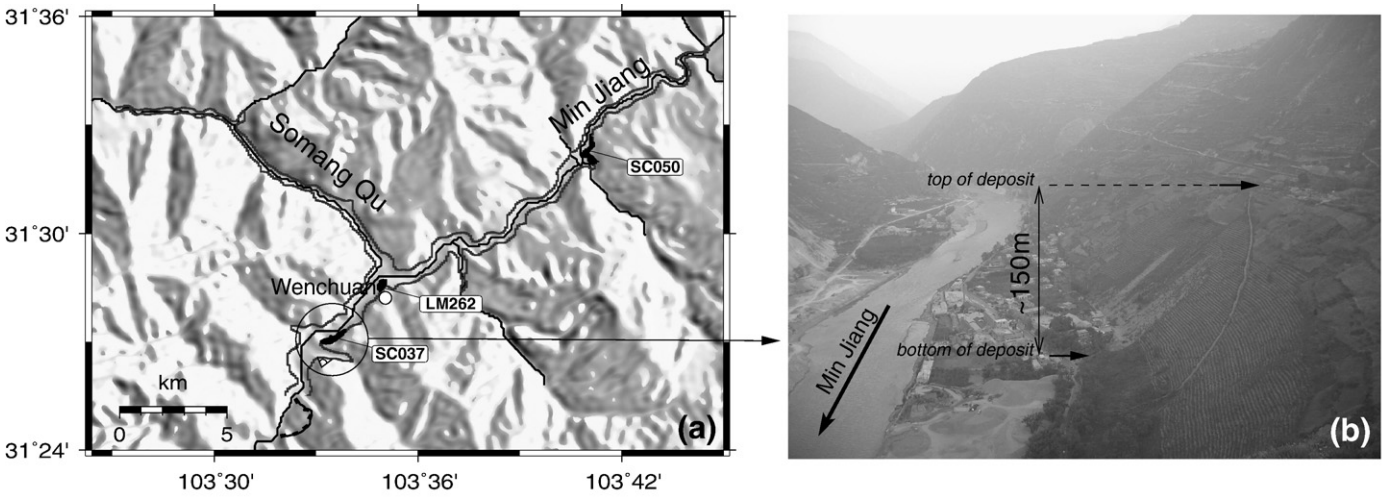

Fig. 6. (a) Localization of lacustrine fill deposits near the town of Wenchuan (black). The dark grey contour indicates the potential extension of the lake and fill sequence, based on the elevation of the top of the deposit surveyed at site SC037. The bold black line indicates the position of the landslide scar. See Fig. 1 for location. (b) View of the complete fill sequence, downstream of Wenchuan.

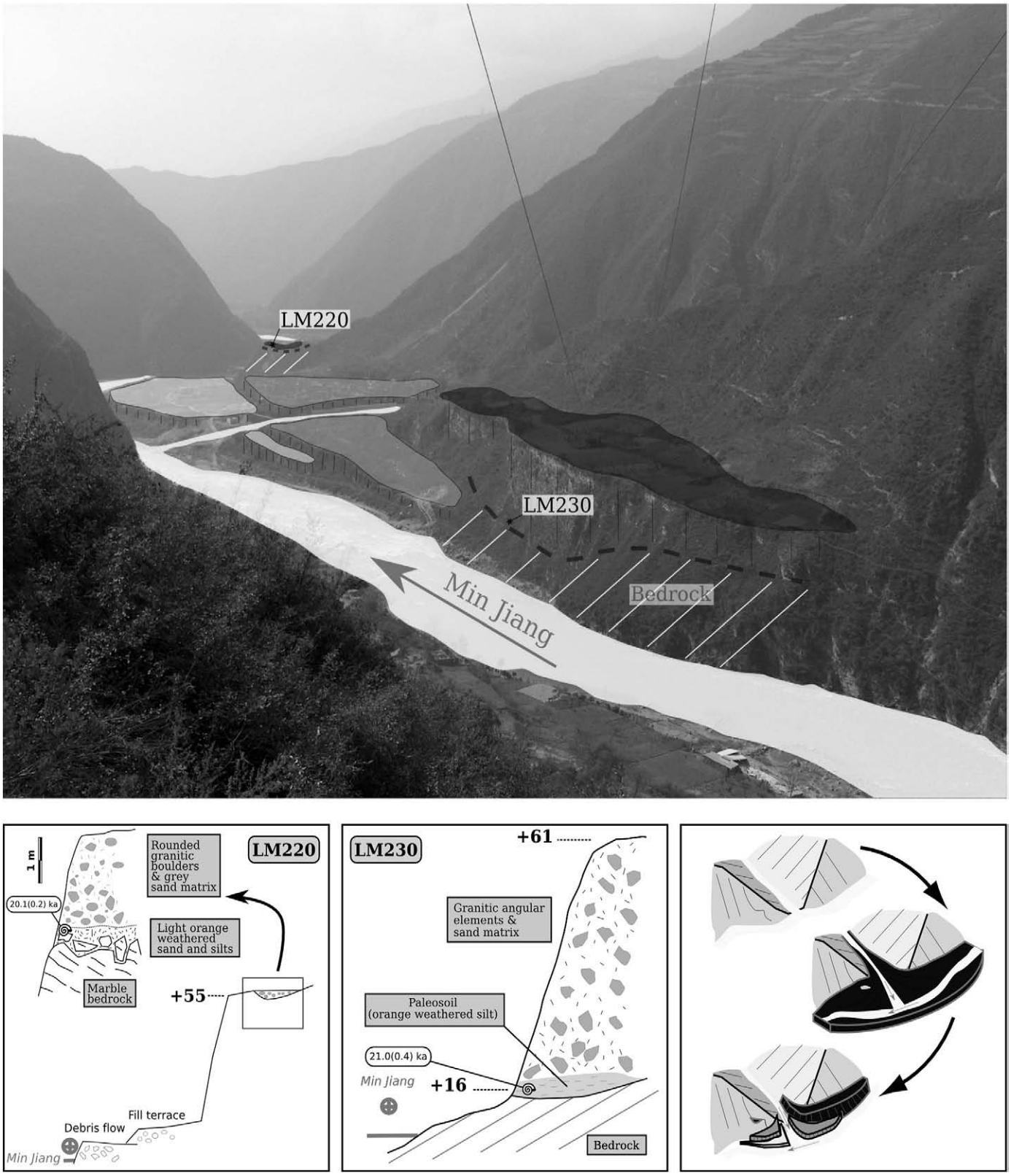

Fig. 7. Configuration of sites LM220 and LM230, lithological description of the fills and possible evolution scenario. See Fig. 1 for situation.

pluton. Gasteropod shells were sampled in paleosols at the base of the deposit in two places (on both sides of the tributary), and give concordant radiocarbon ages of 20.1 ± 0.2 ka BP (LM220) and 20.8 ± 0.4 ka BP (LM230). If we consider the lowermost recorded elevation of the paleotopography of ~16 m, at site LM230, to be an upper limit for the height of the river at the time of emplacement of the alluvial fan we obtain a local maximal incision rate of 0.8 mm/year. The two above examples illustrate the fact that important volumes of sediment can be stored in the river network during several ka and then flushed out during reincision events.

Small remnant abrasion surfaces are locally present along the Min Jiang, principally where the river cuts deep and narrow gorges into the resistant basement units of the Pengguan massif. One of those surfaces was surveyed at site LM264 (Fig. 1). It is located on a steep valley flank, approximately 45 m above the present river, and consists of a narrow fluvial polished surface, with almost no alluvial cover. Cosmogenic dating gives an exposure age of $\sim 3.5 \pm 2$ ^{10}Be ka (Table 2). This young age implies a local incision rate at this location that would be greater than 10 mm/year. While temporary shielding by alluvial or colluvial formations cannot be ruled out, one likely explanation for this young CRN exposure age is that the surface was cut during the active incision of a transient deposit in the valley, either a massive alluvial fill, or a landslide dam. Those observations confirm that the sediment transport and bedrock incision along the Min Jiang, like in many other active mountains (e.g. Lavé and Avouac, 2001; Pratt-Sitaula et al., 2004; Ouimet et al., 2007) is dominated by similar mechanisms, with a succession of discontinuous deposition events (landslides dams, debris flow, and aggradation), followed by rapid reincision of poorly consolidated deposits. From that point of view, the incision rate proposed above can be interpreted as a rate of incision of the river inside those short-lived and unconsolidated deposits, either of alluvial or colluvial origin.

As illustrated with the results presented above, terrace record and also good exposures are scarce and difficult to survey in the Central Longmen Shan. In addition, due to uncertainties associated with dating and/or sites geometries those rates are often upper limits, i.e. maximum incision rates. Globally, the terrace records indicate that fluvial incision rates in the frontal Longmen Shan or along the Min Jiang have been most likely less than 0.8 mm/year over the late Quaternary. Our terrace data only provide local estimates for fluvial incision, for a limited set of locations. In order to further discuss the spatial patterns of denudation we develop a complimentary approach based on present river geometry that provides a more continuous picture of fluvial incision.

4. Fluvial shear stress as a proxy for incision intensity

4.1. Theoretical background

Current proposed models for the evolution of river beds can be classified using two end-member formulations. Some models referred to as transport-limited consider that channel evolution is dependent on the capacity of the stream to carry away its own sedimentary load (Whipple and Tucker, 2002). On the other hand, detachment-limited formulations consider that channel incision is limited by the rate of detachment of rock particles from the river bed, and is independent of sediment discharge (Howard et al., 1994). In most cases the approach used is based on simplified assumptions for the derivation of the incision law, even if models with stronger physical backgrounds, like mixed-tools model, have been recently proposed (Sklar and Dietrich, 2004).

Derivation of most formulations leads to an expression of fluvial incision as a function of channel slope and drainage area, as long as rivers are at equilibrium with tectonics and drain terrains with uniform uplift and erodibility. From the functional form of these different models, it is generally considered that detachment-limited models are sensitive to local uplift and erodibility. On the contrary transport-limited as well as mixed-tools models will be almost insensitive to a sudden change in underlying rock uplift rate or in erodibility, but rather to those variables at the regional scale through their modulation of the sediment flux that transit in a river (e.g. Whipple and Tucker, 2002). In all cases, and despite large differences in behavior, a higher fluvial shear stress exerted by a river on its channel bottom will qualitatively correspond to higher erosion capacity of the river either by an increase in its hydraulic power (detachment-limited models) or by an increase in its transport capacity and bedrock exposure to erosion processes (transport-limited and mixed-tools model).

The fluvial shear stress is defined as

$$\tau = \rho g R S, \tag{1}$$

where ρ is the water density, g is gravitational acceleration, R is the hydraulic radius and S is the stream slope. For streams with large width-to-depth ratio, R is close to the flow depth H, and using the depth-averaged flow velocity U, through mass-conservation and Manning's equation, the shear stress can be recast as a function of channel slope and water discharge Q,

$$\tau = \rho g \frac{(Q \cdot N)^{\frac{3}{5}} S^{\frac{7}{10}}}{W^{\frac{3}{5}}}, \tag{2}$$

where W is the channel width, and N the channel roughness. In a second step, after considering shear stress as a qualitative proxy, and following Kirby et al. (2003), we will consider here that the fluvial incision is mostly detachment-limited in the Central Longmen Shan. We make the hypothesis that the incision rate I of the river is proportional to the shear stress τ in excess of a threshold value (Lavé and Avouac, 2001), such as,

$$I = K(\tau^* - \tau_c^*), \tag{3}$$

where K is the erodibility coefficient, mainly related to lithological properties of the bedrock. τ^*, called Shield stress, represents a dimensionless form of the shear stress such that $\tau^* = \tau/(\Delta\rho g D_{50})$ with $\Delta\rho$ the difference in density between the bedload sediments and the water, and D_{50} the characteristic size not exceeded by 50% of the bedload mass. By using the second approach, we will try to account for the resistance to fluvial processes of the dominant lithologies outcropping in the Central Longmen Shan. We note that the catastrophic sediment input and channel perturbations associated with large earthquakes may affect some of the underlying hypotheses and may complicate the use of fluvial shear stress and incision as proxies for tectonic uplift. However, a similar approach have been applied to river systems in mountainous terrains prone to earthquake induced landsliding such as the Himalayas of central Nepal (Lavé and Avouac, 2001) and it has yielded incision rates that compare reasonably well with long-term or short-term denudation rates (Godard et al., 2004; Garzanti et al., 2007).

4.2. Controlling parameters on shear stress calculations

4.2.1. Discharge

Spatial variations of precipitation rate are relatively limited over the studied watersheds, with an average value of 0.8 mm/year (New et al., 2002). We relate the 10-year return discharge Q_{10} to area A as $Q_{10} \alpha A^{0.85}$ (Lavé and Avouac, 2001). Mean monsoon discharge is estimated to be $\sim 1000\ m^3/s$ at the entry of the Min Jiang in the Sichuan Basin (Qin et al., 2006). We assume a relative uncertainty of 25% on our discharge calculations.

4.2.2. Channel slope, width and sediment size

The channel network was extracted from a 90 m DEM, made of a blend of SRTM and Chinese topographic data. Several steps of treatment and filtering were applied to the raw channel elevation data in order to remove artifacts, such as pits, and extract meaningful long-wavelength information. We consider a relative uncertainty of 20% on our slope calculations.

The bankfull width available for the channel to accommodate a given discharge modulates the intensity of basal processes responsible for bedrock lowering (Lavé and Avouac, 2001; Finnegan et al., 2005). Bankfull channel geometries were digitized for the main rivers of the

Table 3
Average erodibility values assigned to the various formations, evaluated from the data presented on Fig. 8.

Formation	Abrasion rate	Erodibility
	%/km	mm/year
Longmen Shan formations		
Mesozoic Sichuan Basin sediments	0.34 ± 0.24	7.3 ± 5.7
Indosinian plutons	0.11 ± 0.04	2.3 ± 1.4
Songpan Garze Triassic flysch	0.33 ± 0.21	7.1 ± 5.0
Paleozoic platform sediments	0.34 ± 0.28	7.5 ± 6.6
Proterozoic basement	0.08 ± 0.08	1.7 ± 2.0
Nepal Himalayas formations		
F1 Gneisses	0.3 ± 0.1	6.5
Siwalik sandstone	3–10	105
Regression slopes converted to erodibility (Fig. 14)		
Pengguan Massif basement		1.6
Paleozoic/Trias sediments		3.2

Flume experiments abrasion values are converted to erodibility using proportionality factors derived from Himalayan F1 Gneisses parameters (Lavé and Avouac, 2001). The regression slopes of Fig. 14 are converted to equivalent erodibility (in the sense of Eq. (3), using a mean pebble diameter of 8 cm to compute the dimensionless shield stress) by multiplication with a factor $a\rho g D_{50} \sim 1330$.

Central Longmen Shan, using SPOT 5 m resolution panchromatic imagery. We assume a relative uncertainty of 5% on the resulting width evaluation.

Sediments carried by the river are the working tools for the incision of the bedrock, but also have a shielding and armouring effect if the transport capacity of the river is exceeded (Sklar and Dietrich, 2004). The size distribution of the elements constituting the bedload has an important controlling effect on fluvial incision (Sklar and Dietrich, 2004). We performed bedload counting on gravel bars at several locations along the surveyed rivers, to evaluate this parameter, following the procedure of Attal and Lavé (2006), according to classical counting methods (e.g. Kellerhals and Bray, 1971). Our data does not allow us to identify any consistent downstream fining or coarsening pattern. For that reason we choose to use constant values for the bedload size parameters, with D_{50} fixed at 7 cm and 10 cm, which are the average values found for the frontal rivers and the Min Jiang respectively (Godard, 2006).

4.2.3. Erodibility and experimental lithological calibration

The influence of bedrock properties on fluvial incision processes is actively debated and investigated (Sklar and Dietrich, 2001; Duval et al., 2004; Attal et al., 2006; Molnar et al., 2007). Lithological variations are difficult to account for in incision formalisms, and bedrock characteristics are often combined into a single opaque dimensional coefficient along with other climatic and hydrologic influences (Stock and Montgomery, 1999; Whipple and Tucker, 1999).

One of the main difficulties that arise when trying to obtain quantitative information on the resistance of rocks to fluvial erosion is that bedrock behavior strongly depends on the scale of observation. At the mineral scale, the resistance is controlled by mineral hardness. At the centrimetric scale, which is the relevant scale for abrasion processes (Sklar and Dietrich, 2001), the strength of the rock is sensitive to the texture of the mineral assemblage or the eventual existence of fabrics such as schistosity. At the metric scale, parameters such as size and orientation of beds, or fracture density of the material may prevail in controlling the resistance to incision processes and lead to a regime dominated by plucking (Weissel and Seidl, 1997; Whipple et al., 2000).

The actual interactions between those different spatial scales are difficult to assess and it is an important obstacle toward the development of physically based models of bedrock resistance.

Along the Himalayan rivers, it was found that empirically derived erodibility coefficients scale relatively well with experimental abrasion rates on rounded fragments of these lithologies (Attal and Lavé, 2006)

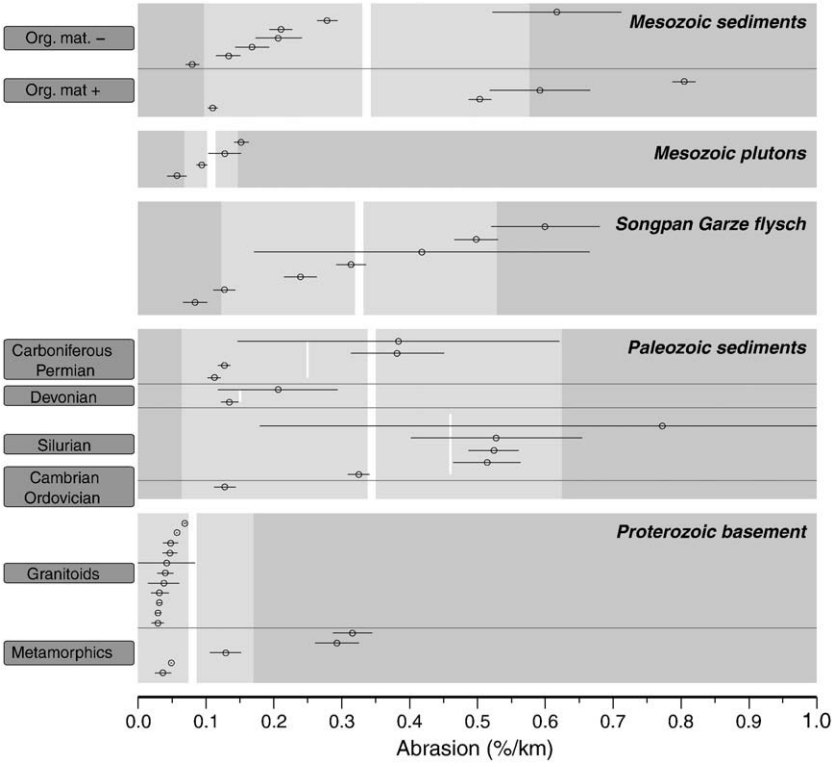

Fig. 8. Abrasion properties (% of mass loss for 1 km transport distance) for samples from the major lithological units in our working area. Error bars represent $\pm\sigma$ for replicate measurements on the same sample. The vertical white thick lines and light grey areas indicate means and $\pm 1\sigma$ interval, respectively, for a whole lithological unit. Vertical thin white lines indicate means for sub-units.

(Table 3), obtained in a circular flume (Attal et al., 2006). Similar abrasion experiments were conducted for lithologies of the Longmen Shan in order to estimate their experimental erodibility by scaling their abrasion rates with those of Himalayan reference units.

For each lithology small spherical samples (2–3 cm) were prepared and carefully rounded. Those samples were then put in the flume with a given amount of reference pebbles. The duration of the experiments ranged from 2 to 5 h, representing a travel distance of 5–12 km. After adequate drying the samples were weighed to quantify the mass loss associated with the abrasion experiment. The lithologies sampled in our study area can be grouped into five distinct tectono-stratigraphic packages, as presented on Fig. 8.

The Proterozoic basement rocks of the Yangtze craton are mainly located in the Pengguan Massif and consist principally in plutonic and metamorphic rocks. Due to their nature those rocks are the most resistant encountered in the Longmen Shan. Proterozoic granitoids exhibit relatively low and homogeneous abrasion rate values, around 0.05%/km (Fig. 8). The resistance of the metamorphic units is more contrasted, and significantly lower than that of the granitic samples. Most of these low resistance samples are metabasalts collected near the Beichuan fault zone, at the contact between the Pengguan Massif and frontal detrital sequence of the Sichuan Basin. This fault zone displays widespread fracturing and schistosity, that lower the strength of the affected rocks.

The Paleozoic platform sediments may present intense cataclasis and schistosity in highly tectonised areas, such as the Wenchuan Fault Zone. Despite the contrasting lithologies encountered in this series most of the units are well consolidated, and with the exception of Silurian levels, present typical abrasion values of 0.2–0.3%/km. Silurian deposits, mainly consisting of detritics and shales, are relatively less resistant.

The Songpan Garze fold belt formation is mainly composed of various types of schist, with highly variable resistance to abrasion, depending on the metamorphic grade. From our abrasion experiments this series can be considered as mildly resistant to erosion. It is to be noted that most of the units of the flysch present important weakness planes defined by the schistosity. Due to the size of our samples the importance of this schistosity is not taken into account in our experiments.

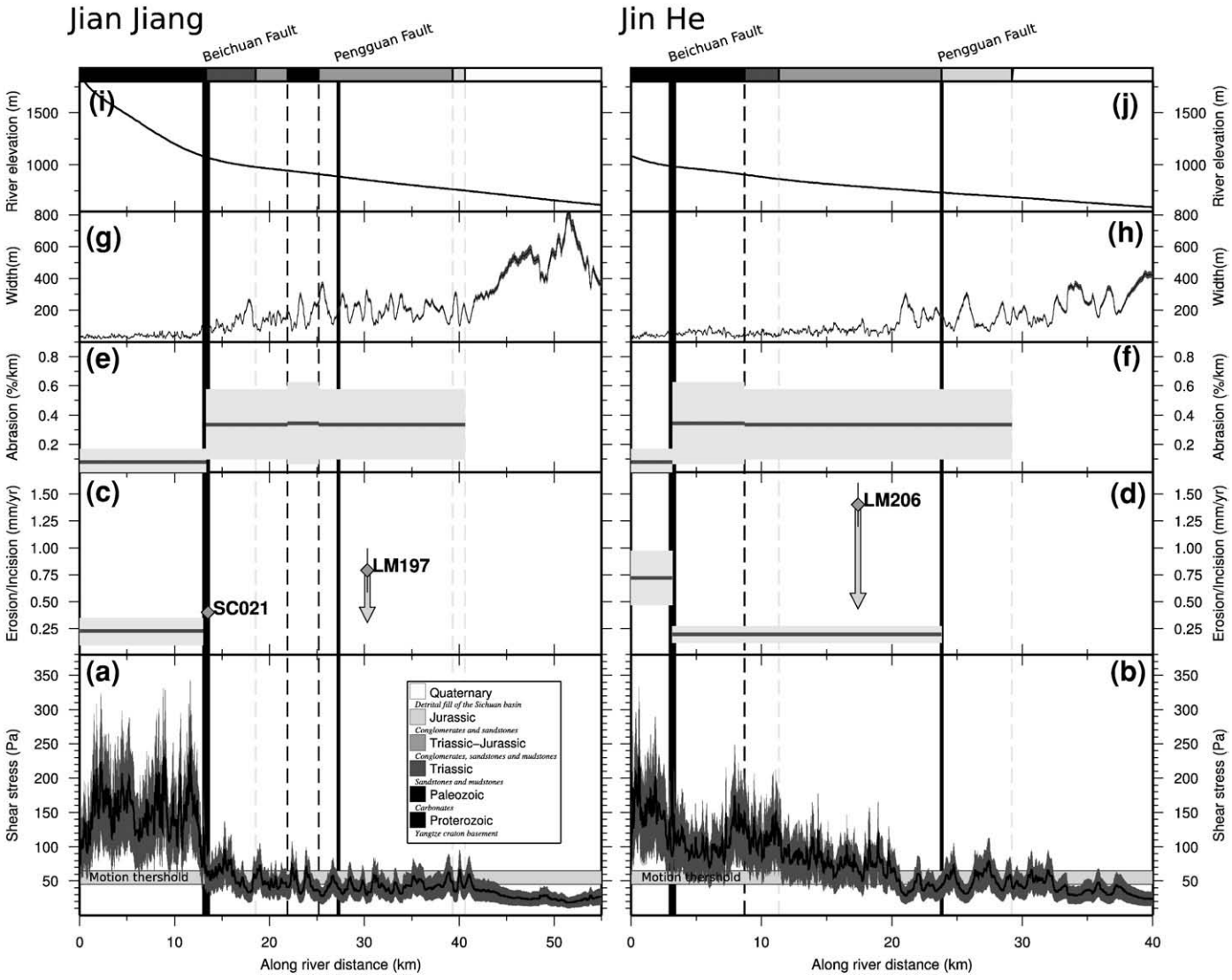

Fig. 9. Compilation of shear stress, erosion/incision rates, erodibility, and river elevation along the Jiang Jiang and Jin He rivers (see Figs. 1, 3 and 4 for situation). Vertical lines indicate faults (dark grey) and geological limits (light grey). Shades of grey in the upper panel indicate geological formations. (a–b) Shear stress profiles along the rivers with cumulative uncertainty (dark grey area). Motion threshold calculated using a D_{50} value of 7 cm. (c–d) Estimation of incision rate (grey diamonds) from terrace surveys. Vertical arrows indicate that the incision rate is a maximum bound. Light grey boxes show average catchment scale erosion rates derived from cosmogenic nuclides concentration in river borne sediments (Table 4 and Figs. 11 and 12). (e–f) Compilation of measured abrasion rates for each formation. (g–h) River width measured from SPOT and Landsat imagery. (i–j) River elevation.

The Indosinian granitic plutons, of Mesozoic age, intrude the Songpan Garze flysch. Their resistance to abrasion is slightly lower than that of the basement granitoids, potentially due to a weak foliation and/or a higher mica content.

The degree of consolidation in the Mesozoic Sichuan Basin formations is variable. From our experiments it appears that the samples containing organic material like small coal veins present significantly higher abrasion rates, which is potentially due to a lowering of the global cohesion of the rock mass by those organic fragments. Mesozoic sandstones and shales are on average more erodible than Paleozoic limestone of the frontal klippes.

More generally, we note that the data from endogenous lithologies present far less scattering than that from sediments. Granitoids present a global cohesion and homogeneity at the sample scale. On the other hand, the existence of heterogeneities for the other lithologies induces contrasting results during the abrasion experiments. Again, the above evaluation of erodibility is based on small-scale abrasion experiments, and does not take into account the large-scale material properties. The erodibility values deduced from our experiments may in particular underestimate the actual, large-scale resistance to erosion of the most fractured lithologies.

4.3. Individual shear stress profiles

Shear stress values are computed from Eq. (2) along streams where terraces were surveyed, i.e. the Min Jiang, the Jian Jiang and the Jin He (Figs. 9 and 10).

The most important variation in shear stress, which can be observed along all the studied rivers, is the transition across the Beichuan Fault where shear stress decreases by a factor ~2–3 in the downstream direction. This feature can be either of tectonic or lithologic origin. Across the Beichuan fault erodibility displays a ~4-fold increase between the resistant Pengguan basement units and the frontal foothills sediments (Figs. 9e–f and 10c). This contrast could account for part of the variation in shear stress, but the uncertainties

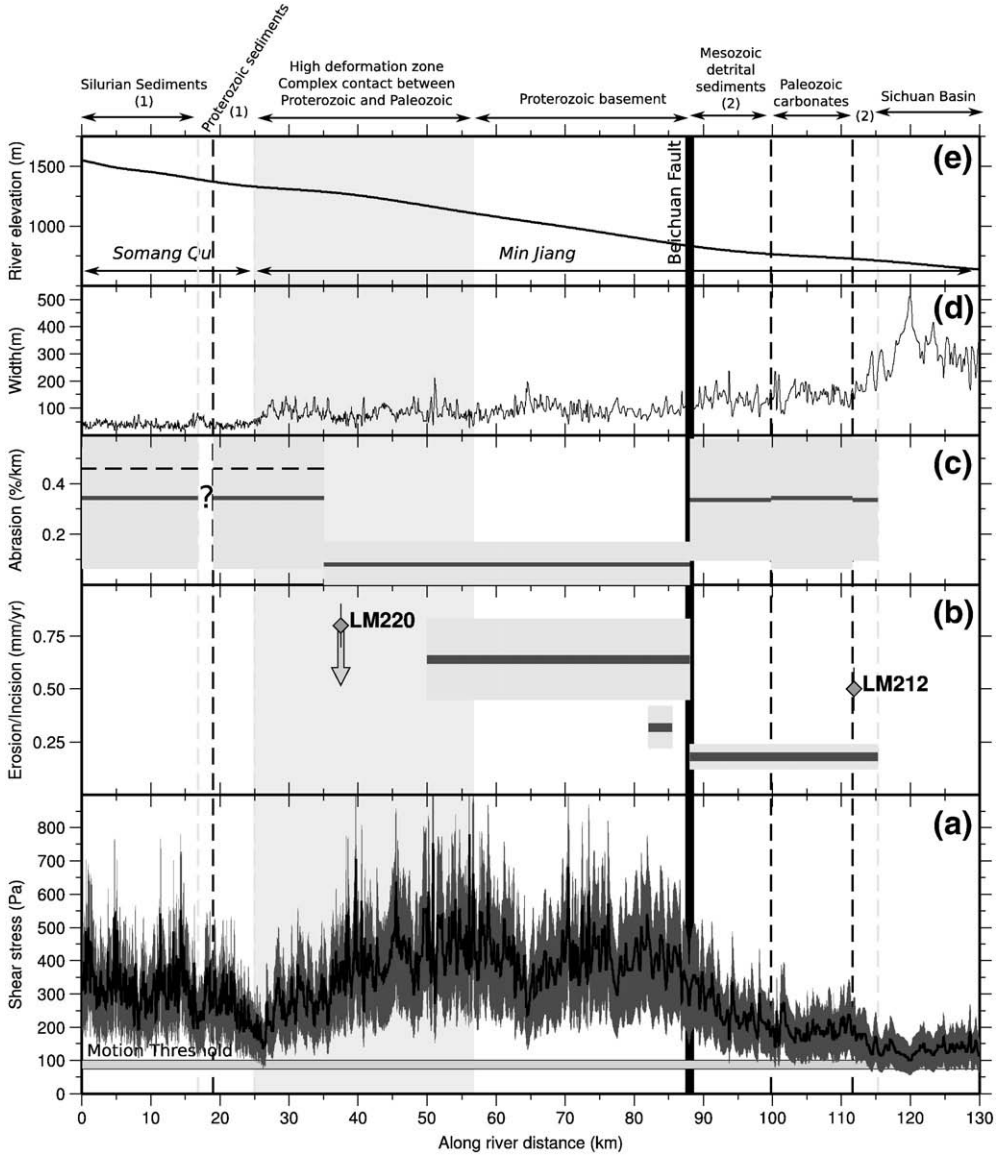

Fig. 10. Compilation of shear stress, erosion/incision rates, erodibility, and river elevation along the Min Jiang river (see Fig. 1 for situation). (a) Shear stress profiles along the river with cumulative uncertainty (dark grey area). Motion threshold calculated using a D_{50} value of 10 cm. (b) Estimation of incision rate (grey diamonds) from terrace surveys. Vertical arrow indicates that the incision rate is a maximum bound. Light grey boxes indicate average catchment scale erosion rates derived from cosmogenic nuclides concentration in river borne sediments (Table 4 and Figs. 11 and 12). (c) Compilation of measured abrasion rates for each formation. The Wenchuan Fault Zone juxtaposes units with contrasting erodibility and also concentrates a large amount of deformation. The erodibility of Silurian formations is slightly higher than the average for the whole Paleozoic units. (d) River width measured from SPOT and Landsat imagery. (e) River elevation.

in our evaluation of a bedrock resistance that would include the role and degree of fracturing are still too large to resolve such ambiguities.

Similarly, large error bars and data scattering in terrace incision rates or erosion rates derived from cosmogenic nuclides in river sands (see the following Section 5) make it difficult to fully attribute the shear stress drop to the existence of differential uplift across the Beichuan Fault (Fig. 9c–d).

On the other hand, observed vertical offset rates of 0.2 mm/year across the Beichuan fault, as recorded by the Late Pleistocene terrace T2 along the Jiang Jiang, suggest that the shear stress drop partly arise from differential uplift. Similarly along the Min Jiang, it can reasonably be proposed that the incision and erosion rates inside the Pengguan Massif are higher than in the foothills (Fig. 10b), and that the shear stress variation across the Beichuan Fault arise from differential tectonic uplift across this structure. In any case, the sharp transition in shear stress across the Beichuan fault clearly indicates that those rivers tend to be, at least locally, in detachment-limited conditions. Transport-limited conditions would indeed imply the river geometry to be mostly unchanged at crossing a lithologic or tectonic boundary (Whipple and Tucker, 2002; Sklar and Dietrich, 2006).

Conversely, the rivers seem to get closer to transport-limited conditions across the frontal foothills since shear stress values are close to bedload motion threshold and since the shear stress profile does not display a sharp drop upon entering the Sichuan basin, but rather a progressive decrease as expected from bedload deposition in the basin and downstream decrease in median bedload size. Such a situation partly invalidates the utilization of shear stress as a proxy for local tectonic uplift, and therefore, makes it difficult to confirm the existence of differential uplift between those two domains, as evidenced from the terrace study. It is to be noted that the shear stress profile along the Jin He might, however, indicates some possible activity across the Pengguan Fault (Fig. 9b).

In the internal part of the range, along the Min Jiang, a slight upstream decrease in shear stress is observed in the Wenchuan Fault Zone, close to the boundary between Pengguan units and Paleozoic sediments. It is therefore tempting to attribute the shear stress change to a lithologic contrast even if the decreased resistance could also arise from the strained and cataclased material of this fault zone. Along the Somang Qu ($x=0$–25 km on Fig. 10) the shear stress values are 50% lower than across the Pengguan massif and coincide with the weaker experimental erodibilities of the Silurian lithologies.

5. Landscape denudation from cosmogenic nuclides

In the previous section we only presented relative estimates of the intensity of incision across our study area. Here, we complement this approach and data by presenting basin-wide absolute erosion rates.

5.1. Principle of cosmogenic measurements in river sands

In situ produced cosmogenic nuclides (CRN) have proved to be a robust and reliable tool for the investigation of the mechanisms and timing of morphological processes (Gosse and Phillips, 2001). In particular the last decade has seen an important development of studies related with the interpretation of the CRN concentration of alluvial sands in eroding landscapes (von Blanckenburg, 2005).

We use the ^{10}Be concentration ([^{10}Be]) in the quartz fraction of sediments, from a particular location, to compute an averaged value for the upstream erosion rate as,

$$\overline{\varepsilon} = \frac{P_0^n \bar{\Lambda}^n + P_0^f \bar{\Lambda}^f + P_0^s \bar{\Lambda}^s}{[^{10}Be]\rho}, \quad (4)$$

where P_0^n, P_0^f and P_0^s are the surface production rates associated with the nucleogenic, fast muons and stopped muons contributions, respectively, while $\bar{\Lambda}^i$ represents the corresponding attenuation factors (Braucher et al., 2003), and ρ is the quartz density.

This approach relies on several assumptions: (1) the typical time scale for the process investigated is short enough to allow us to neglect the influence of radioactive decay for ^{10}Be, (2) the contribution of the different formations of the catchment is homogeneous for the considered mineral phase, and (3) there is no long-term transient storage of sediment inside the hydrographic network (Brown et al., 1995).

5.2. Methods

Active alluvial sediments have been sampled in several localities in the lower Min Jiang watershed, and in the small catchments draining the frontal part of the range (Table 4 and Figs. 11 and 12). Pure quartz was extracted for ^{10}Be determination following the chemical procedure described by (Brown et al., 1991). ^{10}Be analyses were performed at the Tandetron Accelerator Mass Spectrometry facility (Gif-sur-Yvette, France). The obtained data were calibrated directly against the National Institute of Standards and Technology standard reference material 4325 by using the values determined by Nishiizumi et al. (2007), which are a ^{10}Be/^{9}Be ratio of $2.79 \pm 0.03 \times 10^{-11}$ and a ^{10}Be half-life of $1.36 \pm 0.07 \times 10^{6}$ years.

In order to determine erosion rates from the ^{10}Be concentrations measured in the quartz fractions, a modern ^{10}Be production rate at sea-level and high-latitude of 4.5 ± 0.3 atoms/g/year was used. This production rate was computed for internal consistency from the data of Stone (2000) according to the conclusions of the published study on absolute calibration of ^{10}Be AMS standards by Nishiizumi et al. (2007).

Average production rates for each catchment were then computed on a 90 m DEM, using, again for internal consistency, the scaling factors proposed by Stone (2000), because, using the atmospheric pressure as a function of altitude, they take into account the physical properties of cosmic ray particle propagation in the atmosphere and include an improved account for the muonic component in the total cosmogenic production.

In addition, in absence of accurate geologic maps including detailed lithologic descriptions, it will be considered that quartz-bearing lithologies are ubiquitous and uniformly distributed in the Longmen Shan. Such a simplified hypothesis could be wrong in particular in Paleozoic units that include important carbonate formations and also in the Pengguan Massif in localities where

Table 4
Cosmogenic nuclide erosion rate data from alluvial sediment samples.

Sample	Drainage area (km^2)	Mean elevation (m)	^{10}Be (10^4 at/g)	Erosion (mm/year)
LM253	1916	3554 ± 867	4.490 ± 0.875	0.64 ± 0.19
LM254	22,309	3492 ± 680	6.034 ± 0.856	0.45 ± 0.11
LM259	5109	3622 ± 752	4.325 ± 1.255	0.68 ± 0.26
LM261	15,737	3524 ± 589	2.707 ± 1.356	1.01 ± 0.60
LM263	21,299	3531 ± 648	6.107 ± 1.260	0.45 ± 0.14
SC004	359	1942 ± 599	6.191 ± 1.559	0.18 ± 0.06
SC016	141	2695 ± 690	7.824 ± 3.507	0.23 ± 0.12
SC031	350	2938 ± 797	2.869 ± 0.722	0.72 ± 0.25
SC033	63	1427 ± 291	3.928 ± 1.096	0.20 ± 0.07
SC049	15,068	3558 ± 557	7.553 ± 1.187	0.37 ± 0.09
SC059	5	1556 ± 234	2.619 ± 0.591	0.32 ± 0.10
SC071	361	2294 ± 765	5.669 ± 1.312	0.25 ± 0.08
SC082	1915	3556 ± 875	4.888 ± 0.919	0.59 ± 0.17
SC086	22,309	3492 ± 680	5.017 ± 1.520	0.54 ± 0.22

^{10}Be analytical uncertainties are based on counting statistics (1σ) and a conservative assumption of 3% variability accelerator response. Production rates were computed for each pixel of 90 m resolution DEM and then averaged over the basin area. A 10% uncertainty is associated to those basin scale production rates, and propagated to the final result. Error bars on basin elevation are $\pm 1\sigma$. We assume a density $\rho = 2.65$ g cm^{-3} for quartz and we use the attenuation coefficients of Braucher et al. (2003).

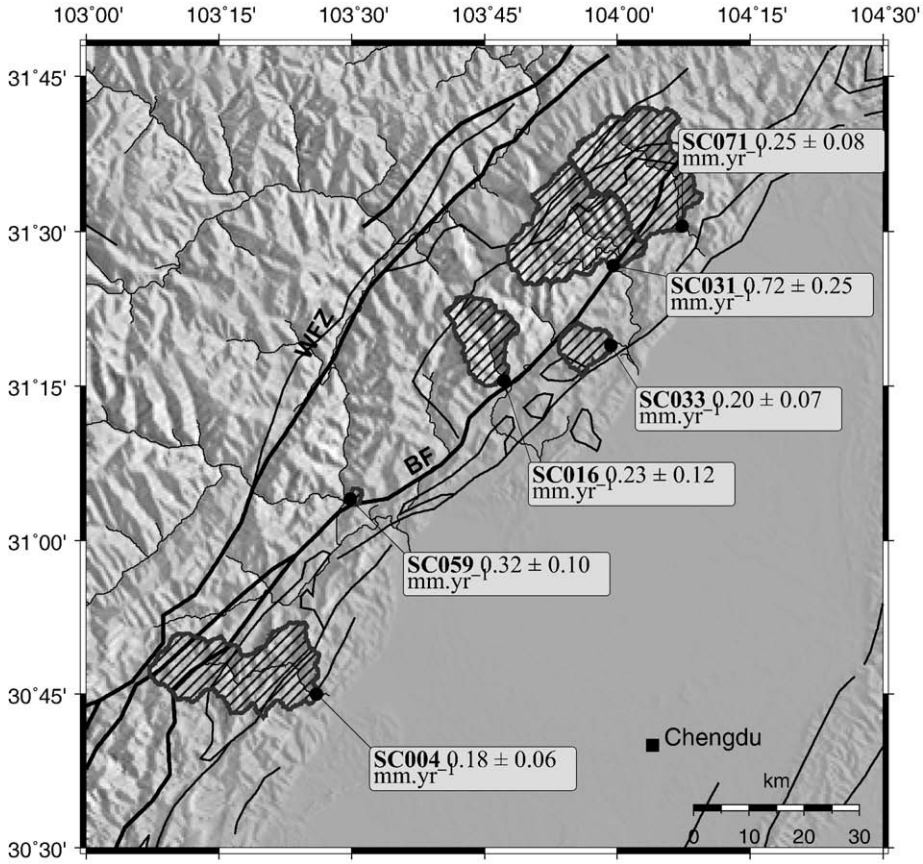

Fig. 11. Distribution of average erosion rates deduced from ^{10}Be concentration of alluvial sediments in the frontal catchments of the Longmen Shan. Black lines indicate the position of the main faults. BF Beichuan Fault. WFZ Wenchuan Fault Zone.

diorites and volcanics are dominant lithologies. Also the size fractions for quartz in sediment derived from the different lithologies may be slightly different, with coarser or finer grains in granitoid-derived or flysch-derived sediments, respectively. We have used the 250–1000 μm fraction in our analyses which is wide enough to substantially mitigate this potential effect.

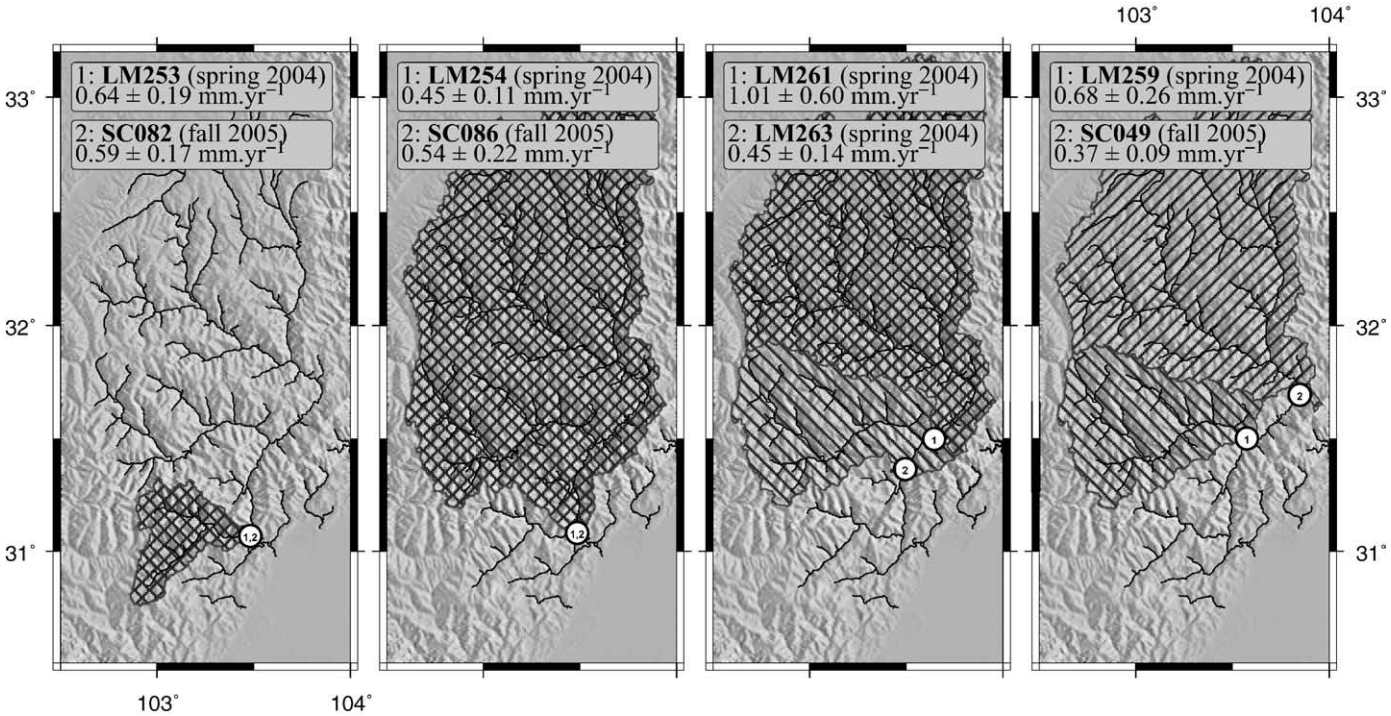

Fig. 12. Distribution of average erosion rates deduced from ^{10}Be concentration of alluvial sediments in the Min Jiang watershed. White dots indicate the locations of the sampling sites, and hatched areas refer to the corresponding watersheds.

5.3. Data

In active and steep mountain ranges, dominated by large landsliding hillslope erosion, it has been forecasted that cosmogenic sand content could overestimate long-term mean erosion rates (Niemi et al., 2005). Those same authors have proposed that mixing effects efficiently dampen the stochastic nature of hillslope sediment delivery by landsliding above a critical catchment area (~100 km^2 for background erosion rates of 1 mm/year). In our study area, most of the sampled basins fulfill the requirement of the above simplified model, and are supposed to provide a representative time-averaging for the erosion rate.

For a few large drainage areas (>1000 km^2), two samples were collected at more than one year interval to test the time variability of the signal (samples LM253, SC082, and LM254, SC086 on Fig. 12). The cosmogenic derived erosion rates in those large-scale basins indeed present a good temporal reproducibility within the limits of the associated uncertainties.

Small basins draining the frontal part of the Longmen Shan (Fig. 11) present mean erosion values that are in the 0.2–0.3 mm/year range, with the exception of sample SC031 (0.72 ± 0.25 mm/year). Despite an insufficient number of samples to draw a robust conclusion, it seems that, on average, the watersheds draining the Pengguan Massif present slightly higher erosion rates (~0.4 mm/year, including SC031) than the ones draining only the frontal thin skin tectonic units (~0.2 mm/year), i.e. in the footwall of the Beichuan Fault. In both cases, those values are lower than the large-scale mean erosion rates of the Min Jiang watershed (Fig. 12), and of the inner part of the range, west of the Pengguan Massif, where erosion rates reach typical values of 0.4–0.7 mm/year, and on average over the whole Min Jiang catchment a value of ~0.5 mm/year (LM254 and SC086). We note that this rate is slightly higher that what has been

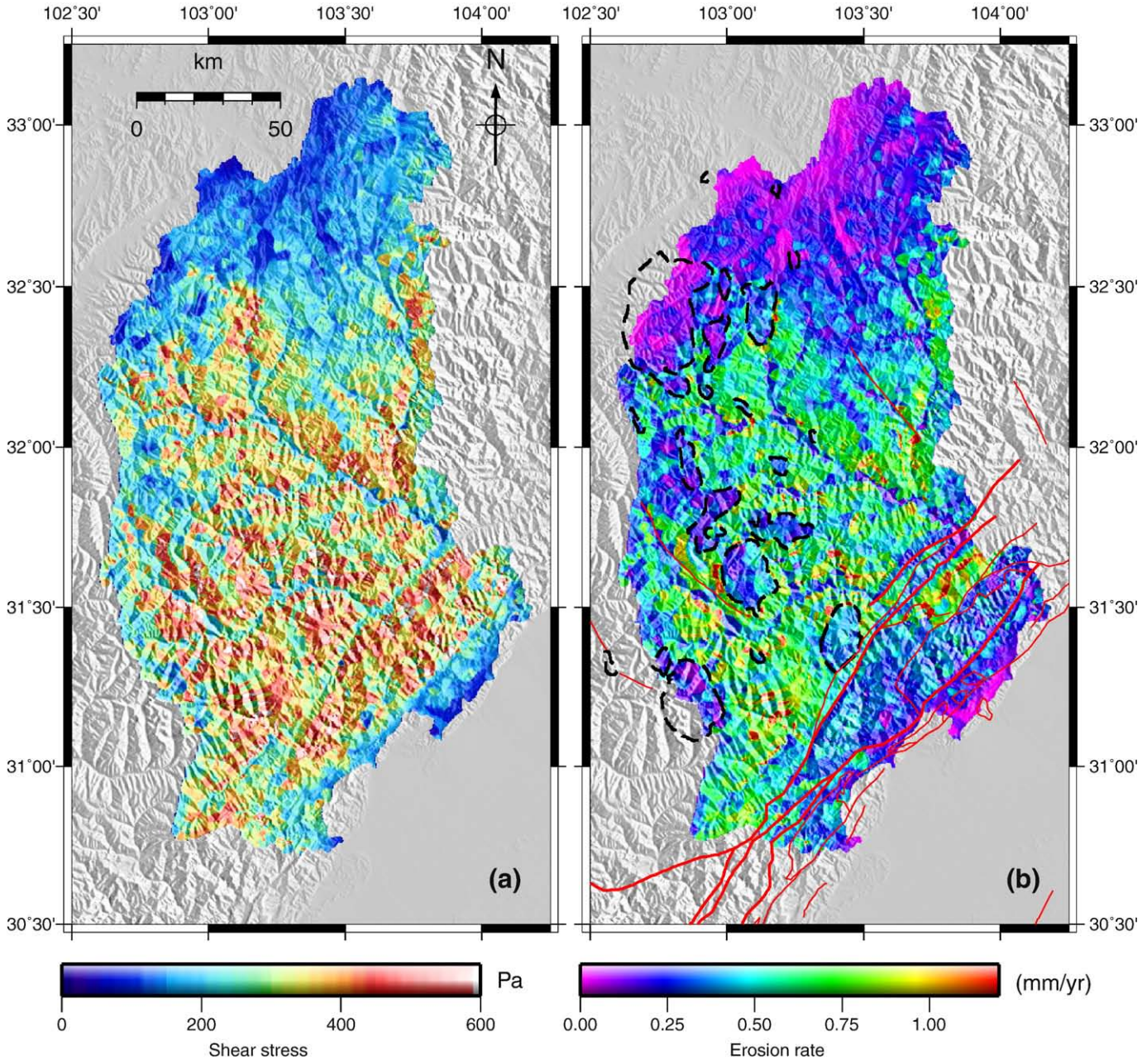

Fig. 13. (a) Interpolated shear stress map for the Min Jiang watershed and selected frontal catchments. (b) Map of mean denudation rates after calibration from Fig. 14. Red lines indicate the position of the major faults. Dashed black lines delineate the major granitic plutons.

obtained by Ouimet et al. (2009) in this area (0.25–0.3 mm/year). Such difference can be explained by the much smaller size of the catchments sampled in their study (<100 km^2), which may eventually lead to an underestimation of the contribution of landsliding to the global erosion of the catchment (Niemi et al., 2005; Yanites et al., 2009). Despite relatively large error bars, the measurements seem to document erosion rates increasing from the northern catchments to the southern ones. However, due to the large size of the upper Min Jiang catchment (SC049), we cannot decipher if such a trend arises from a real southward increase in the erosion rates just west of the Wenchuan Fault Zone, or if it simply relates to the large proportion of low relief regions in the upstream weakly dissected Tibetan surfaces of the upper Min Jiang catchment.

Another important point that should be kept in mind when interpreting those erosion rates is the influence of sediment inputs by massive co-seismic landsliding similar to what has been observed after the May 2008 earthquake. The recurrence time of those events is at least a few ka and likely >5 ka (Burchfiel et al., 2008; Godard et al., 2009a), which is significantly longer than the integration time for the ^{10}Be derived erosion rates (~1.5 ka). The erosion contribution of such events is not fully taken into account in our erosion rates which may be lower than the actual long-term values.

6. Regional map for shear stress and denudation

6.1. Approach and scope

Most of our previous observations are focused on the external part of the margin. In order to expand our view of the spatial distribution of erosion further west, we have adopted a more regional approach of the shear stress model by computing shear stress all along the fluvial network and then interpolating in between to derive a fluvial incision map. Following the approach of Lavé and Burbank (2004), shear stress calculations were extended to the whole drainage network up to a source area of ~5 km^2 (Fig. 13a), upstream of which debris slope effects dominate channel erosion. These values defined on the stream network were then interpolated on the whole working area in order to smooth the high frequency noise due mostly to DEM imperfections and produce a continuous visual representation of this parameter that allows the discussion of spatial variations. To compute shear stress, the same procedure as for single river profiles (Section 4) was followed except for median grain size, here considered as uniform and equal to 8 cm. Systematic measurement of channel width is a difficult task that requires intensive field surveys or a large amount of high-resolution imagery. For that reason many models of channel evolution estimate channel width W through the hypothesis that there exists a scaling relationship between width and discharge. On the basis of the digitized bankfull channel geometries along the Min Jiang and Somang Qu rivers, least square inversion was performed to propose the following scaling relationship for width, channel slope S and contributing area A,

$$W = 2.3A^{0.38}S^{\sim 0},\ (r^2 = 0.79). \quad (5)$$

According to our data, channel width appears to be statistically independent from slope. This is substantially different from the results of Finnegan et al. (2005) as it does not predict a narrowing of the river along steeper reaches. Our inversion only includes data from two river segments for which we have high-resolution imagery. We acknowledge that it may result in a sampling bias leading to an underestimation of shear stress for locally steepened reaches. However, if such bias exists, we are confident that it only affect small-scale localized features and allow us to derive the large-scale shear stress pattern. For the rivers draining across the frontal foothills this relationship implies an underestimation of the actual width.

In the following step, using average erosion rates from river sand, we perform a tentative empirical calibration of the erodibility coefficient in Eq. (3) in order to derive a regional map of the denudation rate on the basis of the shear stress map (Fig. 13a). We also compare those calibration coefficients with previous measurements of terrace incision rates (Figs. 9 and 10) and long-term exhumation rates (Godard et al., 2009a). For each of the basins where average erosion rates were derived from cosmogenic concentration measurements we compute an average shear stress value, assuming that on average hillslopes are equilibrated with their adjacent segment of the fluvial network. Based on the experimental erodibility values (Table 3), we distinguish three main large-scale lithologic domains: the Pengguan Massif and Indosinian plutons, the frontal foothills sediments, and the Paleozoic and Triassic units located farther west in the Min Jiang watershed (Fig. 1).

This dataset is presented in Fig. 14. We compute weighted regression lines that go through an average critical shear stress

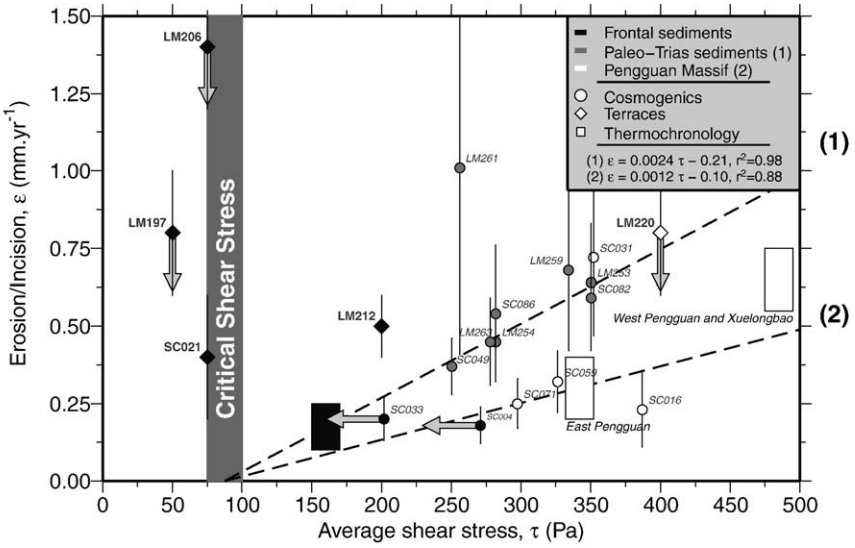

Fig. 14. Comparison of basin-averaged shield stress values and denudation rate from terraces, thermochronology and ^{10}Be measurements in alluvial sediments for the frontal units, the Pengguan units and the Paleozoic/Triassic units. The vertical grey arrows indicate that the incision rates at the specified locations are probably maximum bounds due to the geometry and geomorphic context of sampling sites (see Section 3 for further details). The horizontal grey arrows indicate that the shear stress values are overestimated due to the use of the regional scaling relationship for channel width in the frontal foothills sediments. The best linear weighted fits through alluvial sands data for the Paleozoic–Triasic units (1) and the Pengguan basement (2) are indicated by the dashed black lines. The linear fits go through the critical shear stress value of 87.5 Pa.

value of ~90 Pa corresponding to pebble threshold motion (Lavé and Avouac, 2001). The Paleozoic and Triassic sedimentary units, and the Pengguan basement units display consistently distinct trends with respective slopes of 0.0024 and 0.0012. It is to be noted first that the calibration clearly displays the effect of lithology on fluvial shear stress. Second, the erodibility coefficients associated with those regression slopes are of the same order as the ones found in the Himalayas (Table 3), giving some credit to the first-order estimate provided by the shear stress model and the experimental abrasion rates performed on the outcropping lithologies. The 2-fold difference between the two coefficients is, however, significantly lower than the 4-fold difference expected from experimental abrasion values (Table 3 and Fig. 8), and unfortunately prevents the use of a direct and linear relationship between our experimental abrasion rates and local erodibility coefficient.

The data from basins that exclusively drain Sichuan Basin folded sediments (SC004 and SC033) display too much scatter to define a consistent regression line through them. This scatter is either due to width underestimation in the shear stress calculation or terrace incision rate overestimation. To overcome such absence of empirical calibration, we will remark that these units present, on average, experimental abrasion rates close to the ones of the Paleozoic and Triassic sedimentary units (Table 3 and Fig. 8), and therefore we will further adopt the same coefficient in these two domains. Due to the similarities in lithologies and abrasion resistance between the Indosinian plutons and the Pengguan basement we use the same calibration parameters for both units.

A direct application of Eq. (3) with those empirical erodibility coefficients allow us to compute Fig. 13b which presents spatially continuous values for erosion over our whole area of interest. Before interpreting those maps, we insist on the fact that there are important uncertainties associated with the estimation of the discharge, as well as local variations in channel width or erodibility that are not encapsulated in the used scaling relationships and mean values. More importantly, as discussed in Section 3, the detachment-limited incision model in itself could be inadequate close to the motion threshold of pebbles, i.e. particularly for the rivers draining the Sichuan Basin folded sediments. We also note that such first-order derivation of erosion may overestimate the influence of short wavelength lithological pattern, such as the observed sharp erosion variations between the small Indosinian plutons and Songpan flysch sediments. As such Fig. 13b should only be used to discuss the long-wavelength pattern of erosion.

6.2. Results

We note the existence of a wide zone (~100 km) of high shear stress values (300–500 Pa) with erosion rates in the 0.5–1 mm/year range located West of the Wenchuan Fault Zone (Fig. 13). The contrast across the Beichuan Fault in between the Pengguan massif and the frontal folded sedimentary series is sharper on the shear stress map than on the erosion map since part of the contrast is due to the difference in erodibility of the two lithologic domains. No significant change in shear stress values can be deciphered across the Wenchuan Fault Zone. This is, in particular, true for areas of equivalent lithologies, on both sides of the fault, such as the Xuelongbao pluton and the Pengguan Massif. Further west, denudation gradually decreases when reaching the headwaters of the Min Jiang, which is not a lithological effect, but is related with the progressive diminution of shear stress values down to <0.1 mm/year in the north-western part of the headwaters. These results argue for a distribution of active denudation that is similar to that proposed by Kirby et al. (2003), with a broad zone of active denudation starting at the topographic front and a progressive westward attenuation. The main differences with the denudation map proposed by Kirby et al. (2003) are that, in our case, (1) erosion rates are significantly lower, (2) the zone of higher denudation is broader and propagates farther to the north-west and (3) using a specific calibration coefficient for the Pengguan Massif lithologies (Fig. 14) leads to relatively low denudation in this area, but we acknowledge that this conclusion is only supported by a limited dataset.

The shear stress and erosion maps, in addition of extending the view on erosion in the western part of the Min Jiang watershed, provide also information on the local structure of erosion and relationships between the different parts of the landscape. In a given region, if uplift and erodibility are uniform, and if fluvial incision is indeed ruled by a detachment-limited law, the shear stress will be uniform as long as the landscape is at equilibrium. Conversely any significant difference in shear stress between the low and the high order stream channels will reflect some disequilibrium: a waxing or waning denudation if high order streams present higher or lower shear stress values than low order streams, respectively. In the north-western part of the Min Jiang watershed, the headwaters of the fluvial network are characterized by a marked diminution in shear stress: the presence of such knickpoint could for example result from an active regressive erosion wave propagating toward the Plateau interior. In contrast, in the middle part of the watershed, shear stress and incision values along higher order drains such as the Min Jiang river and its major tributaries are often significantly lower than along their lower order tributaries. This could potentially indicate some progressive waning denudation in the large rivers, after a wave of regressive erosion had passed through them, meanwhile it's still propagating along the smaller tributaries. In both cases, the shear stress pattern strongly suggests that the Min Jiang watershed is characterized by significant local disequilibrium between uplift and erosion.

7. Discussion

7.1. Spatial and temporal distribution of denudation rates in the Longmen Shan

The methods we used to estimate erosion rates in the Longmen Shan encompass distinct time scales. However, they all provide a general pattern indicating that erosion rates are lower than 1 mm/year all over that region, in close correspondence with the subdued tectonic activity of this Tibetan margin (Table 5 and Fig. 15). The denudation rates derived from the available thermochronological datasets, in particular from the exhumation of the 10 Ma paleo-Partial Retention Zone for radiogenic Helium in zircons (Godard et al., 2009a), indicate that such low rates have been on average prevalent in

Table 5
Compilation of denudation rates (mm/year) for the major morpho-structural units of the Longmen Shan, at different time scales.

	Frontal foothills	Eastern Pengguan Massif	WFZ and Western Pengguan Massif	Upper Min Jiang drainage
Long-term denudation (several Ma) Low-temperature thermochronology	0.1–0.25 (?)	~0.65 (down to 0.3 recently)	~0.65	<0.6
Intermediate term (several 10 ka) Terrace incision	<0.5–0.8	?	<0.8	?
Short term (several ka) CRN in river sands	~0.2	0.4 (0.2–0.7)	0.6 (?)	0.5

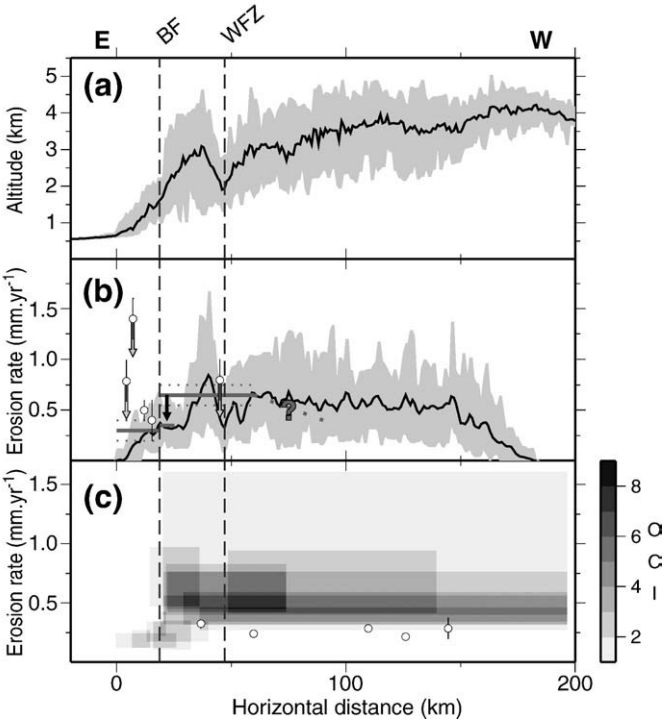

Fig. 15. Comparison of different methods for the estimation of denudation rates across the Longmen Shan. Position of the N315 cross section is indicated on Fig. 1. (a) Mean, max and min topography, swath width is 100 km. (b) Black curve and grey envelopes indicate the mean, min and max values of erosion (Fig. 13b), swath width is 40 km. Those erosion values are integrating a lower lithological calibration coefficient for the Pengguan Massif and do not take into account the long-term effects of landsliding. Therefore they should be considered as a minimum (see text for discussion). Dark grey thick lines are the exhumation rates for the main structural units of the range, inferred from the reconstruction of the zircon-He PRZ (Godard et al., 2009a) on the basis of available data (Arne et al., 1997; Kirby et al., 2002; Richardson et al., 2008; Godard et al., 2009a). Dotted lines display estimated ranges of variation. Black vertical arrow shows the possible decrease in exhumation since 3 Ma in the Eastern Pengguan Massif. White dots indicate the estimation of incision rates obtained from terraces surveys in this study. Vertical grey arrows signify that the values are maximum bounds. (c) Projection of the basin-wide averaged erosion rates derived from ^{10}Be measurements on alluvial sediments (Figs. 11 and 12). Each measurement is represented by a box whose dimensions are set according to the watershed extension and the confidence interval of the average erosion rate estimate. Overlapping Confidence Intervals (OCI) are obtained by stacking those individual basins confidence ranges. White circles are rates of erosion from (Ouimet et al., 2009).

the region since the Late Miocene. We note that those rates are significantly lower than the 1–2 mm/year inferred by Kirby et al. (2002, 2003) in the same area, that were derived from a limited number of isolated thermochronological samples.

With the exception of two incision rates in the foothills (LM197 and LM206) that are clearly higher than both short-term and long-term denudation rates and correspond to maximum values, all the datasets indicate the existence of a narrow zone of slow erosion (<0.5 mm/year) in the frontal part of the Longmen Shan and a broader area of higher erosion (0.4–1 mm/year) in the hinterland. This area of higher erosion rates seems to culminate west of the Wenchuan Fault Zone according to the incision map and cosmogenic dating of river sands, even if the sampling strategy for river sediments adopted in this study does not allow us to document the spatial variations in erosion rate intensity west of the Pengguan Massif. For the incision map, this conclusion is, however, dependent on the low erodibility coefficient calibrated for the resistant Pengguan Massif (Fig. 14). Using the same coefficient for all the units would lead to a transition between the low and high erosion zone located farther east, closer to the Beichuan fault. Concerning the erosion in the frontal range and Pengguan Massif it is also important to consider the influence of regular co-seismic landsliding. Due to the long recurrence time for large earthquakes in this area, this effect is not integrated in the erosion rates derived from cosmogenic nuclides. For that reason the erosion rates that are derived from those measurements may underestimate the actual long-term erosion of the frontal range. The volume of sediments produced by the May 2008 Sichuan earthquake and similar events is currently unconstrained, so it is not possible to quantitatively discuss their actual contribution, but it should be pointed out that the erosion values proposed on Fig. 15 are most likely minimum estimates for the areas within distances <100 km from the Beichuan fault. At last, whereas the comparison of the values for the southern major Min Jiang tributaries (LM253, SC082 and LM259) and the upper northern portion of the Min Jiang watershed (SC049) suggest a northward decrease in erosion rate, it is not possible to confirm the spatial pattern of this decrease close to the headwaters that is inferred from shear stress distribution or to some extent by the reduced set of thermochronology data in this region (Arne et al., 1997; Kirby et al., 2002).

The broad-scale analysis of the distribution of incision processes across the margin suggests that a wide zone of active denudation is located at the Plateau margin, as proposed by Kirby et al. (2003). The observations that shear stress (1) decreases dramatically when approaching the northern headwaters of the catchment and (2) is significantly lower across the higher order drains close to the base level, may indicate the existence of a disequilibrium inside the fluvial network. Godard et al. (2009a) have proposed that a possible explanation for the westward decrease of the exhumation ages across the Longmen Shan could be the existence of a transient wave of regressive erosion propagating across the margin. The pattern displayed by the shear stress and erosion maps (Fig. 13) would suggest that this erosional wave has already travelled through the main streams of the Min Jiang watershed, that it is actively acting in the low order streams of the middle part of the watershed, but that it has not yet reached the farther headwaters in the northern part of the watershed. This hypothesis of a transient evolution of the topographic step, with a progressive displacement of active erosion from southeast to northwest, toward the Plateau interior is also supported by the erosion distribution inside the Pengguan Massif (Fig. 13b). The eastern flank of the Pengguan Massif, that would react first to any uplift of the Tibetan eastern margin relative to the Sichuan basin, is presently eroding slower than the western flank, which drains into the middle Min Jiang river >50 km upstream of its outlet in Sichuan basin and would be affected later by a wave of regressive erosion. The shear-stress-derived erosion rates are ~40% lower along the eastward draining watersheds in the Pengguan Massif than the westward draining ones. U–Th/He apatite ages (Godard et al., 2009a) also indicate that denudation rate has probably slowed down by a factor ~2 during the Plio-Pleistocene relative to the Late Miocene on the most eastern and frontal part of the Pengguan Massif while it remained roughly unchanged across the Xuelongbao pluton in the most internal part for the same period of time.

Finally, it is to be noted that the high range of the Longmen Shan experienced more long-term denudation than the other parts located East or West (Kirby et al., 2002; Godard et al., 2009a), resulting in the exhumation of the mid-crustal basement core of thePengguan Massif, which presents the most resisting lithologies in our working area (Fig. 8). The arrival at the surface of those highly resistant lithologies may have strongly modified the erosion dynamics in the Central Longmen Shan. Schlunegger and Simpson (2002) have pointed out that such decrease in the erosional efficiency during the exhumation of basement units may have strongly impacted the evolution of the European Alps. Here, we suspect that once those resistant Proterozoic granitoids and metamorphics have reached the surface, the time scale of erosional relaxation of the margin may have significantly changed. The transition from the Paleozoic sediments to those basement rocks represents a 2 to 4 fold decrease in erodibility according to our

empirical calibration and experimental abrasion rates respectively. We propose that this progressive exhumation of resistant lithologies in the high range of the Longmen Shan could in part explain the sustainment of the abrupt topographic margin and the existence of >4500 m summits in this area.

7.2. Fault activity across the Longmen Shan

In many morphotectonic studies, despite the clear distinction that has to be made between rock uplift and denudation (England and Molnar, 1990), it is common to interpret denudation rates in term of rock uplift rates assuming that uplift and erosion are balanced, or at local scale to interpret difference in denudation rates across a fault in terms of vertical throw rates. Even if we previously saw that the studied area is probably affected by some large-scale disequilibrium, we also assume in the following that at the local scale similar elements of the landscape (for example streams of same order) on both sides of a fault are equilibrated and that some estimation of the vertical throw rates for such faults can be inferred from the difference in erosion rates between the two compartments.

The multi-scale erosion pattern obtained here is consistent with the existence of a sustained differential uplift between the foothills and the Sichuan basin. Such differential uplift could potentially be associated with thrusting across the Pengguan Fault (Densmore et al., 2007), which has also been activated during the Sichuan Earthquake, and/or to folding of the most frontal anticlines. According to the incision and erosion rates, the uplift rate would range between 0.2 and 0.5 mm/year across the frontal foothills.

The Beichuan Fault is the major structure that has accommodated most of the deformation since 10 Ma according to thermochronologic data (Arne et al., 1997; Kirby et al., 2002; Burchfiel et al., 2008; Godard et al., 2009a). Thrust activity across this fault would be associated with an important exhumation event of the Pengguan Massif that started at that time. The activity of the Beichuan fault is difficult to discuss on the basis of the erosion data presented here: first the cosmogenic dating on river sand display a large scattering for the basins draining the eastern flank of the Pengguan Massif, second the erosion contrast derived from the shear stress values strongly depends on the relative calibration of the lithologic erodibility in the footwall and hangingwall of the fault (Figs. 8 and 14), which, as we pointed previously, should be handled with caution. According to the faulted terrace T2 along the Jiang Jiang (see Section 1 and Densmore et al. (2007)), the vertical throw rate is at least of 0.2 mm/year and more if distributed on several fault branches at the surface. On the basis of cosmogenic dating on river sands, the differential erosion rates on both sides of the Beichuan Fault would range between 0.1 and 0.6 mm/year.

Our erosion data suggests comparable amounts of partitioning of the thrust activity on the Beichuan Fault and frontal foothill faults. Thermochronologic data, on the other hand, indicates that the long-term throw rates are 2–3 times lower on foothill faults than on Beichuan Fault (Godard et al., 2009a). However the large uncertainties do not allow to conclude if this expresses some recent evolution of the thrusting activity. Finally as a matter of comparison, field investigations of the distribution of vertical displacement, after the May 2008 Sichuan seismic rupture in the Central Longmen Shan, suggest that the slip on Beichuan Fault may have been 1–3 times larger than on the Pengguan Fault (Lin et al., 2009).

According to the above data, and assuming a dip angle of 30° to 50° for the Beichuan Fault at depth as given by focal solutions of the recent Sichuan seismic event (USGS, 2008), the mean vertical differential uplift rate of 0.4 mm/year across the fault leads to an associated slip rate of 0.5–0.8 mm/year at depth (i.e. below the point where the decolement below the foothill is probably branching). Given that the average dip slip component of the $M_w \sim 7.9$ rupture reaches ~5 m along the Pengguan massif (Ji and Hayes, 2008), the recurrence time of an earthquake of this magnitude would be larger than 6000 years. Finally, as already noted in Section 2, no clear changes in either shear stress or erosion occur between the Pengguan and Xuelongbao massifs, on both sides of the Wenchuan Fault Zone. It is consistent with the long-term kinematics inferred by Godard et al. (2009a) from low-temperature thermochronology, who propose that no important differential exhumation occurred across the structure since 10 Ma. This also contradicts some conceptual models that postulate that normal activity of the Wenchuan Fault Zone has a central role in the exhumation of the Longmen Shan as a response to deep crustal forcing (Burchfiel, 2004; Meng et al., 2006).

7.3. Implications for Eastern Tibet tectonics and geodynamics

One of the most striking features of the Longmen Shan range is the coexistence of low shortening in the upper crust as seen by geodesy (King et al., 1997; Chen et al., 2000; Shen et al., 2005; Gan et al., 2007) and high topographic gradients with >4500 m-high summits. This situation leads to at least two questions: does this topography represent some inherited topography from a previous period during which tectonic activity was higher, promoting the thickening and uplift of the Longmen Shan margin, or conversely is the present topography in equilibrium with tectonic forces? And in that second case what kind of tectonic model can maintain such a topographic step without major horizontal shortening?

One of the most recent models proposes to answer both questions by the propagation of lower crustal material inside a narrow channel, driven by a pressure gradient from the Plateau to the foreland (Clark et al., 2005). The material flux would be deviated by the rigid core of the Yangtze craton, and part of it forced upward, which would result in surface uplift in the Longmen Shan through large-scale topographic inflation. We can, however, not rule out that the above mentioned paradox, between high topographic gradients and low convergence, may only be an apparent one. Indeed, Godard et al. (2009a) have underlined that the exhumation rates for the Pengguan Massif, inferred from low-temperature thermochronology, are consistent with slow convergence driven by thrusting activity on the Beichuan fault, with horizontal convergence rates ≤ 1 mm/year that are compatible with current geodetic estimates within error bars. The associated rock uplift rate is ~0.5 mm/year range which is consistent with the erosion rates inferred in this study, and the Longmen Shan mountains would be as many as other “classical” mountain ranges associated to present thrusting activity. In such a latter case, only the presence at surface of highly resistant lithologies, such as the Pengguan Massif basement rocks, could explain, in our opinion, the existence of a high and steep topography at pace with subdued thrusting rates. We note that recent studies by Hubbard and Shaw (2009) have documented the shortening history of the frontal range and also point to a dominant contribution of upper-crustal deformation to the building of the range.

On the other hand, we previously noticed that the studied region does not seem to be at equilibrium and that many erosional features could correspond to the propagation of a regressive wave of erosion after a tectonic building event. Among the possible mechanisms to explain such a tectonic event and initial margin uplift, which in the case of the Longmen Shan would have began around 10 Ma ago, it can been proposed: (1) the sequential step-wise propagation of deformation and Plateau uplift northward (Tapponnier et al., 2001), (2) the Late Miocene convective removal of lithospheric mantle driving Tibetan surface uplift (Molnar et al., 1993) or (3) the thickening of the crust by mid or lower crustal injection (Zhao and Morgan, 1987; Clark and Royden, 2000), sometime in the past (without a necessary dynamic support by an active diverging channel flow (Clark et al., 2005)).

Observations on present denudation processes and rates do not allow discrimination between the different scenarios for initial plateau uplift, since all would be affected by a similar transient

regressive denudation pattern propagating across the uplifted margin. In addition, numerical models by Godard et al. (2009b) support the idea that, in the absence of convergence, erosion-triggered deep crustal processes can contribute to topographic stability in such settings of plateau margin. Self-parallel retreat of the topographic margin can both explain the persistence over several Ma of a sharp topographic step between the Sichuan basin and the Tibetan Plateau, and also the existence of thrusting activity on the faults at the base of the topographic step like the Beichuan Fault and the foothill faults in response to mass removal by erosion.

In all the above cases, it can again be argued that the exhumation of highly resistant basement lithologies like those of the Pengguan Massif has certainly contributed to lengthen the evolution timescale of the topographic front, and helped to maintain high and steep topography. This could constitute a part of the explanation for the persistence of significant gradients across the Longmen Shan margin, even if the major topographic building episode occurred several Ma ago.

According to the short-term erosion data presented in this paper, and to the long-term exhumation data provided by low-temperature thermochronology (Arne et al., 1997; Kirby et al., 2002; Godard et al., 2009a), we suggest that the present topographic step represents some inherited topography from a Late Miocene–Pliocene period during which tectonic activity was higher than today. Even if there is still tectonic shortening across this margin or some dynamic support, the denudation pattern of the Longmen Shan would be made by a combination of this subdued tectonic activity with inherited relaxation pattern. Future higher precision geodetic data, as well as more details on the distribution of long-term and recent denudation, will help to decipher the relative contribution of recent and inherited tectonic imprints in controlling the geodynamic evolution of the Longmen Shan range.

8. Conclusions

We have documented denudation across the Longmen Shan with a set of methods that provide complimentary access to different space and time scales as well as different resolutions. We have identified a spatial denudation pattern characterized by slow erosion in the frontal range and headwaters and higher erosion West of the Beichuan Fault. While this pattern is globally consistent with that proposed by Kirby et al. (2003) we also note the existence of evidence for a transient relaxation contribution in the denudation of the margin. At maximum, erosion rates are between 0.5 and 1 mm/year and <0.5 mm/year in the frontal range. Our observations support the existence of thrusting activity across the range, accommodated by the Beichuan Fault and also by frontal structures such as the Pengguan Fault. Even if the approaches we used do not allow us to assess the magnitude of strike slip deformation on those structures, our inferences provide some insights on the seismotectonic context of the May 2008 Sichuan Earthquake.

Plateau margins are dynamic features that go through cycles of construction and degradation. The general process of margin erosion involves the establishment of gradients in surface processes between the foreland and the plateau, with displacements of active denudation areas, progressive dissection of unaffected regions and important transitions in erosional regime (Liu-Zeng et al., 2008). The timescale of such evolution can be significantly modulated by lithological contrasts, and in particular the exhumation of resistant basement units, like for example the Pengguan Massif in our region of interest. The Longmen Shan range, along the Eastern border of the Tibetan Plateau, is subjected to such transient evolution, with a geomorphic context controlled by both the slow shortening and uplift across the Beichuan Fault and the progressive westward propagation of erosion.

Acknowledgments

This work was funded by an INSU-Relief grant and the ANR ContinentDyn. Chengdu University of Technology staff provided assistance in the organization of the field work. An earlier version of this paper benefited from thorough comments and syntax corrections by G. B. Fisher. Constructive reviews by two anonymous reviewers greatly helped to improve the manuscript. Most of the illustrations were prepared using the Generic Mapping Tools (GMT) software (Wessel and Smith, 1995).

References

An, Z., Kutzbach, J.E., Prell, W.L., Porter, S.C., 2001. Evolution of Asian monsoons and phased uplift of the Himalayan Tibetan plateau since Late Miocene times. Nature 411, 62–66.
Armijo, R., Tapponnier, P., Mercier, J.L., Tonglin, H., 1986. Quaternary extension in southern Tibet. J. Geophys. Res. 91, 13803–13872.
Arne, D., Worley, B., Wilson, C., Chen, S.F., Foster, D., Luo, Z.L., Liu, S.G., Dirks, P., 1997. Differential exhumation in response to episodic thrusting along the eastern margin of the Tibetan Plateau. Tectonophys 280 (3–4), 239–256.
Attal, M., Lavé, J., 2006. Changes of bedload characteristics along the Marsyandi River (central Nepal): implications for understanding hillslope sediment supply, sediment load evolution along fluvial networks and denudation in active orogenic belts. In: Willett, S.D., Hovius, N., Brandon, M.T., Fischer, D. (Eds.), Tectonics, Climate, and Landscape Evolution: Geol. Soc. Am. Spec. Pap, vol. 398, pp. 143–171.
Attal, M., Lavé, J., Masson, J.P., 2006. New facility to study river abrasion processes. J. Hydraul. Eng. 132 (6), 624–628.
Avouac, J.P., 2003. Mountain building, erosion, and seismic cycle in the Nepal Himalaya. Adv. Geophys. 46.
Beaumont, C., Fullsack, P., Hamilton, J., 1992. Erosional control of active compressional orogens. Thrust Tectonics. Chapman & Hall, pp. 1–18.
Beaumont, C., Jamieson, R.A., Nguyen, M.H., Lee, B., 2001. Himalayan tectonics explained by extrusion of a low viscosity crustal channel coupled to focused surface denudation. Nature 414, 738–742.
Bookhagen, B., Burbank, D.W., 2006. Topography, relief, and TRMM-derived rainfall variations along the Himalaya. Geophys. Res. Lett. 33, 08405.
Braucher, R., Bourlès, D.L., Colin, F., Brown, E.T., Boulange, B., 2003. Brazilian laterite dynamics using in situ-produced Be-10. Earth Planet. Sci. Lett. 163, 197–205.
Brown, E.T., Edmond, J.M., Raisbeck, G.M., Yiou, F., Kurz, M.D., Brook, E.J., 1991. Examination of surface exposure ages of Antarctic moraines using insitu produced Be-10 and Al-26. Geochim. Cosmochim. Act. 55 (8), 2269–2283.
Brown, E.T., Stallard, R.F., Larsen, M.C., Raisbeck, G.M., Yiou, F., 1995. Denudation rates determined from the accumulation of in situ-produced Be-10 in the Luquillo experimental forest, Puerto-Rico. Earth Planet. Sci. Lett. 129, 193–202.
Burbank, D.W., Leland, J., Fielding, E., Anderson, R.S., Brozovic, N., Reid, M.R., Duncan, C., 1996. Bedrock incision, rock uplift and threshold hillslopes in the northwestern Himalayas. Nature 379, 505–510.
Burchfiel, B.C., 2004. New technology: new geological challenges. GSA Today 14, 4–10.
Burchfiel, B.C., Chen, Z., Liu, Y., Royden, L.H., 1995. Tectonics of the Longmen Shan and adjacent regions, Central China. Int. Geol. Rev. 37, 661–735.
Burchfiel, B., Royden, L., van der Hilst, R., Hager, B., Chen, Z., King, R., Li, C., Lu, J., Yao, H., Kirby, E., 2008. A geological and geophysical context for the Wenchuan earthquake of 12 May 2008, Sichuan, People's Republic of China. GSA Today 18, 4–11.
Cattin, R., Avouac, J.-P., 2000. Modeling mountain building and the seismic cycle in the Himalaya of Nepal. J. Geophys. Res. 105 (B6), 13389–13407.
Chen, S.F., Wilson, C.J.L., 1996. Emplacement of the Longmen Shan Thrust-Nappe belt along the eastern margin of the Tibetan plateau. J. Struct. Geol. 18 (4), 413–430.
Chen, Z., Burchfiel, B.C., Liu, Y., King, R.W., Royden, L.H., Tang, W., Wang, E., Zhao, J., Zhang, X., 2000. Global Positioning System measurements from eastern Tibet and their implications for India/Eurasia intercontinental deformation. J. Geophys. Res. 105 (B7), 16215–16227.
Clark, M.K., Royden, L.H., 2000. Topographic ooze: building the eastern margin of Tibet by lower crustal flow. Geology 28 (8), 703–706.
Clark, M.K., Schoenbohm, L.M., Royden, L.H., Whipple, K.X., Burchfiel, B.C., Zhang, X., Tang, W., Wang, E., Chen, L., 2004. Surface uplift, tectonics, and erosion of Eastern Tibet from large-scale drainage patterns. Tectonics 23 (1), 1006.
Clark, M.K., Bush, J.W.M., Royden, L.H., 2005. Dynamic topography produced by lower crustal flow against rheological strength heterogeneities bordering the Tibetan Plateau. Geophys. J. Int. 162 (2), 575–590.
Coleman, M., Hodges, K., 1995. Evidence for Tibetan plateau uplift before 14-myr ago from a new minimum age for east–west extension. Nature 374 (6517), 49–52.
Danzeglocke, U., Jöris, O., Weninger, B. 2008. CalPal-2007online. http://www.calpal-online.de.
Densmore, A.L., Ellis, M.A., Li, Y., Zhou, R.J., Hancock, G.S., Richardson, N., 2007. Active tectonics of the Beichuan and Pengguan faults at the eastern margin of the Tibetan Plateau. Tectonics 26 (4), 4005.
Dong, S., Zhang, Y., Wu, Z., Yang, N., Ma, Y., Shi, W., Chen, Z., Long, C., An, M., 2008. Surface rupture and co-seismic displacement produced by the Ms 8.0 Wenchuan Earthquake of May 12th, 2008. Sichuan, China: eastwards growth of the Qinghai–Tibet Plateau. Acta Geol. Sin. 82, 938–948.

Dunne, J., Elmore, D., Muzikar, P., 1999. Scaling factors for the rates of production of cosmogenic nuclides for geometric shielding and attenuation at depth on sloped surfaces. Geomorphology 27, 3–11.
Duval, A., Kirby, E., Burbank, D., 2004. Tectonic and lithologic controls on bedrock channel profiles and processes in coastal California. J. Geophys. Res. 109 (F3), F03002.
England, P., Houseman, G., 1989. Extension during continental convergence with application to the Tibetan Plateau. J. Geophys. Res. 94 (B12), 17561–17579.
England, P., Molnar, P., 1990. Surface uplift, uplift of rocks, and exhumation of rocks. Geology 18, 1173–1177.
Fielding, E., Isacks, B., Barazangi, M., Duncan, C., 1994. How flat is Tibet? Geology 22 (2), 163–167.
Finnegan, N.J., Roe, G., Montgomery, D.R., Hallet, B., 2005. Controls on the channel width of rivers: implications for modeling fluvial incision of bedrock. Geology 33, 229–232.
Gan, W., Zhang, P., Shen, Niu Z., Wang, M., Wan, Y., Zhou, D., Cheng, J., 2007. Present-day crustal motion within the Tibetan Plateau inferred from GPS measurements. J. Geophys. Res. 112, B08416.
Garzanti, E., Vezzoli, G., Andò, S., Lavé, J., Attal, M., France-Lanord, C., DeCelles, P., 2007. Quantifying sand provenance and erosion (Marsyandi River, Nepal Himalaya). Earth Planet. Sci. Lett. 258 (3–4), 500–515.
Godard, V., 2006. Couplage érosion-tectonique en contexte de convergence intracontinentale. Étude comparée de la chaîne Himalayenne et des Longmen Shan (est-Tibet). Ph.D. thesis, Université Paris XI — École Normale Supérieure.
Godard, V., Cattin, R., Lavé, J., 2004. Numerical modelling of mountain building: interplay between erosion law and crustal rheology. Geophys. Res. Lett. 31, L23607.
Godard, V., Pik, R., Lavé, J., Tibari, B., Cattin, R., de Sigoyer, J., Pubellier, M., Zhu, J., 2009a. Late Cenozoic evolution of the Central Longmen Shan (Eastern Tibet), insight from (U–Th)/He thermochronometry. Tectonics 28, TC5009.
Godard, V., Cattin, R., Lavé, J., 2009b. Erosion control on the dynamics of low-convergence-rate continental plateaus margins. Geophys. J. Int. 179 (2), 763–777. doi:10.1111/j.1365-246X.2009.04324.x.
Gosse, J.C., Phillips, F.M., 2001. Terrestrial in situ cosmogenic nuclides: theory and application. Quat. Sci. Rev. 20 (14), 1475–1560.
Harrowfield, M.J., Wilson, C.J.L., 2005. Indosinian deformation of the Songpan Garze Fold Belt, northeast Tibetan Plateau. J. Struct. Geol. 27 (1), 101–117.
Hay, W.W., Soeding, E., DeConto, R.M., Wold, C.N., 2002. The Late Cenozoic uplift: climate change paradox. Int. J. Earth Sci. 91 (5), 746–774.
Howard, A.D., Dietrich, W.E., Seidl, A., 1994. Modeling fluvial erosion on regional to continental scales. J. Geophys. Res. 99 (B7), 13971–13986.
Huang, M.H., Buick, I.S., Hou, L.W., 2003. Tectonometamorphic evolution of the Eastern Tibet Plateau: evidence from the central Songpan-Garze Orogenic Belt, western China. J. Petrol. 44 (2), 255–278.
Hubbard, J., Shaw, J.H., 2009. Uplift of the Longmen Shan and Tibetan plateau, and the 2008 Wenchuan (M = 7.9) earthquake. Nature 458, 194–197.
Ji, C., Hayes, G. 2008. Preliminary result of the May 12, 2008 MW 7.9 eastern Sichuan earthquake. http://earthquake.usgs.gov.
Kellerhals, R., Bray, D.I., 1971. Sampling procedures for coarse fluvial sediments. J. Hydraul. Eng. 97, 1165–1180.
King, R.W., Shen, F., Burchfiel, B.C., Royden, L.H., Wang, E., Chen, Z., Liu, Y., Zhang, X.-Y., Zhao, J.-X., Li, Y., 1997. Geodetic measurments of crustal motion in southwest China. Geology 25 (2), 179–182.
Kirby, E., Reiners, P.W., Krol, M.A., Whipple, K.X., Hodges, K.V., Farley, K.A., Tang, W.Q., Chen, Z.L., 2002. Late Cenozoic evolution of the eastern margin of the Tibetan Plateau: inferences from Ar-40/Ar-39 and (U–Th)/He thermochronology. Tectonics 21 (1), 1001.
Kirby, E., Whipple, K.X., Tang, W.Q., Chen, Z.L., 2003. Distribution of active rock uplift along the eastern margin of the Tibetan Plateau: inferences from bedrock channel longitudinal profiles. J. Geophys. Res. 108 (B4), 2217.
Lavé, J., Avouac, J.-P., 2000. Active folding of fluvial terraces across the Siwaliks hills, Himalaya of central Nepal. J. Geophys. Res. 105 (B3), 5735–5770.
Lavé, J., Avouac, J.-P., 2001. Fluvial incision and tectonic uplift across the Himalayas of central Nepal. J. Geophys. Res. 106 (B11), 26561–26591.
Lavé, J., Burbank, D.W., 2004. Denudation processes and rates in the Transverse Ranges, southern California: erosional response of a transitional landscape to external and anthropogenic forcing. J.Geophys. Res. 109 (F1), 01006.
Lin, A., Ren, Z., Jia, D., Wu, X., 2009. Co-seismic thrusting rupture and slip distribution produced by the 2008 Mw7.9 Wenchuan earthquake, China. Tectonophysics 471 (3–4), 203–215. doi:10.1016/j.tecto.2009.02.014.
Liu-Zeng, J., Tapponnier, P., Gaudemer, Y., Ding, L., 2008. Quantifying landscape differences across the Tibet plateau: implications for topographic relief evolution. J. Geophys. Res. accepted. doi:10.1029/2007JF000897.
Liu-Zeng, J., et al., 2009. Co-seismic ruptures of the 12 May 2008, Ms 8.0 Wenchuan earthquake, Sichuan: east–west crustal shortening on oblique, parallel thrusts along the eastern edge of Tibet. Earth Planet. Sci. Lett. doi:10.1016/j.epsl.2009.07.017.
Mattauer, M., Malavieille, J., Calassou, S., Lancelot, J., Roger, F., Hao, Z.W., Xu, Z.Q., Hou, L.W., 1992. The Songpan-Garze Triassic belt of West Sechuan and Eastern Tibet: a décollement fold belt on passive margin. C. R. Acad. Sci. 314 (6), 619–626.
Meng, Q.R., Hu, J.M., Wang, E., Qu, H.J., 2006. Late Cenozoic denudation by large-magnitude landslides in the eastern edge of Tibetan Plateau. Earth Planet. Sci. Lett. 243 (1–2), 252–267.
Molnar, P., Tapponnier, P., 1975. Cenozoic tectonics of Asia: effects of a continental collision. Science 189, 419–426.
Molnar, P., England, P., Martinod, J., 1993. Mantle dynamics, uplift of the Tibetan Plateau, and the Indian monsoon. Rev. Geophys. 31 (4), 357–396.
Molnar, P., Anderson, R.S., Anderson, S.P., 2007. Tectonics, fracturing of rock, and erosion. J. Geophys. Res. 112 (F3), 03014.
New, M., Lister, D., Hulme, M., Makin, I., 2002. A high-resolution data set of surface climate over global land areas. Climate Res. 21 (1), 1–25.
Niemi, N.A., Oskin, M., Burbank, D.W., Heimsath, A.M., Gabet, A.M., 2005. Effects of bedrock landslides on cosmogenically determined erosion rates. Earth Planet. Sci. Lett. 237 (3–4), 480–498.
Nishiizumi, K., Imamura, M., Caffee, M.W., Southon, J.R., Finkel, R.C., McAninch, J., 2007. Absolute calibration of ^{10}Be standards. Nucl. Instrum. Methods B 52, 403–413.
Ouimet, W.B., Whipple, K.X., Royden, L.H., Sun, Z.M., Chen, Z.L., 2007. The influence of large landslides on river incision in a transient landscape: eastern margin of the Tibetan Plateau (Sichuan, China). Geol. Soc. Am. Bull. 119, 1462–1476.
Ouimet, W.B., Whipple, K.X., Granger, D.E., 2009. Beyond threshold hillslopes: channel adjustment to base-level fall in tectonically active mountain ranges. Geology 2009 (37), 579–582.
Pratt-Sitaula, B., Burbank, D.W., Heimsath, A., Ojha, T., 2004. Landscape disequilibrium on 1000–10, 000 year scales Marsyandi River, Nepal, central Himalaya. Geomorphology 58 (1–4), 223–241.
Qin, J., Huh, Y., Edmond, J.M., Du, G., Ran, J., 2006. Chemical and physical weathering in the Min Jiang, a headwater tributary of the Yangtze River. Chem. Geol. 227, 53–69.
Raymo, M.E., Ruddiman, W.F., 1992. Tectonic forcing of late Cenozoic climate. Nature 359, 117–122.
Reimer, et al., 2004. IntCal04 terrestrial radiocarbon age calibration 26–0 ka BP. Radiocarbon 46, 1029–1058.
Richardson, N.J., Densmore, A.L., Seward, D., Fowler, A., Wipf, A., Ellis, M.A., Yong, L., Zhang, Y., 2008. Extraordinary denudation in the Sichuan Basin: insights from low-temperature thermochronology adjacent to the eastern margin of the Tibetan Plateau. J. Geophys. Res. 113, B04409.
Royden, L.H., Burchfiel, B.C., King, R.W., Wang, E., Chen, Z.L., Shen, F., Liu, Y.P., 1997. Surface deformation and lower crustal flow in Eastern Tibet. Science 276, 788–790.
Royden, L.H., Burchfiel, B.C., van der Hilst, R.D., 2008. The geological evolution of the Tibetan plateau. Science 321, 1054–1058.
Schlunegger, F., Simpson, G., 2002. Possible erosional control on lateral growth of the European Central Alps. Geology 30, 907–910.
Shen, Z.K., Lu, J.N., Wang, M., Bürgmann, R., 2005. Contemporary crustal deformation around the southeast borderland of the Tibetan Plateau. J. Geophys. Res. 110, B11409.
Sklar, L.S., Dietrich, W.E., 2001. Sediment and rock strength controls on river incision into bedrock. Geology 29 (12), 1087–1090.
Sklar, L.S., Dietrich, W.E., 2004. A mechanistic model for river incision into bedrock by saltating bed load. Water Resour. Res. 40 (6), 06301.
Sklar, L.S., Dietrich, W.E., 2006. The role of sediment in controlling steady-state bedrock channel slope: implications of the saltation–abrasion incision model. Geomorphology 82 (1–2), 58–83.
Stock, J.D., Montgomery, D.R., 1999. Geologic constraints on bedrock river incision using the stream power law. J. Geophys. Res. 104 (B3), 4983–4993.
Stone, J.O., 2000. Air pressure and cosmogenic isotope production. J. Geophys. Res. 105, 23753–23759.
Stuiver, M., Reimer P. J., Reimer R. W. 2005. CALIB 5.0. (WWW program and documentation).
Tapponnier, P., Xu, Z.Q., Roger, F., Meyer, B., Arnaud, N., Wittlinger, G., Yang, J.S., 2001. Oblique stepwise rise and growth of the Tibet plateau. Science 294, 1671–1677.
Thatcher, W., 2007. Microplate model for the present-day deformation of Tibet. J. Geophys. Res. 112 (B1), B01401.
U.S. Geological Survey, 2008. National Earthquake Information Center. http://earthquake.usgs.gov.
von Blanckenburg, F., 2005. The control mechanisms of erosion and weathering at basin scale from cosmogenic nuclides in river sediment. Earth Planet. Sci. Lett. 237, 462–479.
Wallis, S., Tsujimori, T., Aoya, M., Kawakami, T., Terada, K., Suzuki, K., Hyodo, H., 2003. Cenozoic and Mesozoic metamorphism in the Longmenshan orogen: implications for geodynamic models of Eastern Tibet. Geology 31 (9), 745–748.
Weissel, J.K., Seidl, M.A., 1997. Influence of rock strength properties on escarpment retreat across passive continental margins. Geology 25 (7), 631–634.
Weninger, B., Jöris, O., 2008. A 14C age calibration curve for the last 60 ka: the Greenland-Hulu U/Th timescale and its impact on understanding the Middle to Upper Paleolithic transition in Western Eurasia. J. Hum. Evol. 55, 772–781.
Wessel, P., Smith, W.H.F., 1995. New version of the Generic Mapping Tools released. EOS Trans. AGU 76, 329.
Whipple, K.X., Meade, B.J., 2004. Controls on the strength of coupling among climate, erosion, and deformation in two-sided, frictional orogenic wedges at steady state. J. Geophys. Res. 109, F01011.
Whipple, K.X., Tucker, G.E., 1999. Dynamics of stream-power river incision model: implications for height limits of mountain ranges, landscape response timescales, and research needs. J. Geophys. Res. 104 (B8), 17661–17674.
Whipple, K.X., Tucker, G.E., 2002. Implications of sediment-flux-dependent river incision models for landscape evolution. J. Geophys. Res. 107 (B2), 22039.
Whipple, K.X., Hancock, G.S., Anderson, R.S., 2000. River incision into bedrock: mechanics and relative efficacy of plucking, abrasion, and cavitation. Geol. Soc. Am. Bull. 112 (3), 490–503.
Willett, S.D., Brandon, M.T., 2002. On steady states in mountain belts. Geology 30, 175–178.
Wilson, C.J.L., Harrowfield, M.J., Reid, A.J., 2006. Brittle modification of Triassic architecture in Eastern Tibet: implications for the construction of the Cenozoic plateau. J. Asian Earth Sci. 27 (3), 341–357.
Worley, B.A., Wilson, C.J.L., 1996. Deformation partitioning and foliation reactivation during transpressional orogenesis, an example from the central Longmen Shan, China. J. Struct. Geol. 18 (4), 395–411.

Yang, Z.X., Waldhauser, F., Chen, Y.T., Richards, P.G., 2005. Double-difference relocation of earthquakes in central-western China, 1992–1999. J. Seismol. 9 (2), 241–264.
Yanites, B.J., Tucker, G.E., Anderson, R.S., 2009. Numerical and analytical models of cosmogenic radionuclide dynamics in landslide-dominated drainage basins. J. Geophys. Res. 114, F01007.
Zhang, P.-Z., Shen, Z., Wang, M., Gan, R., Bürgmann, R., Molnar, P., Wang, Q., Niu, Z., Sun, J., Wu, J., Hanrong, S., Xinzhao, Y., 2004. Continuous deformation of the Tibetan Plateau from Global Positioning System data. Geology 32, 809–812.
Zhao, W.L., Morgan, W.J., 1987. Injection of Indian crust into Tibetan lower crust: a two-dimensional finite element model study. Tectonics 6, 489–504.